NTNU – Trondheim
Norwegian University of
Science and Technology

State and parameter identification applied to dual gradient drilling with oil based mud

Dag Slettebø

Master of Science in Cybernetics and Robotics
Submission date: June 2015
Supervisor: Ole Morten Aamo, ITK
Co-supervisor: Espen Hauge, Statoil

Norwegian University of Science and Technology
Department of Engineering Cybernetics

Problem Description

Deepwater drilling is challenging business. After Macondo, the industry has been stimulated to come up with new solutions improving safety. The past few years, the costs of drilling wells have increased significantly while the oil price has dropped. To stay in business and to be able to drill planned wells in a profitable manner, both safety and efficiency have to be improved. Managed Pressure Drilling (MPD) for floaters is a technology, where rig time spent on handling wellbore instabilities, such as kicks and losses, can be reduced. Accurate control of the downhole pressures enables drilling through narrow drilling windows with reduced risk of taking an influx or going on varying degrees of losses.

After gaining operational experience with dual gradient drilling (DGD), field data has become available. This field data gives the opportunity to validate mathematical models and estimate unknown parameters. Once a verified model has been established, it can be used to experiment with controller design and tuning. This will ease controller tuning offshore, which in turn saves valuable rig time.

Goal: Find a mathematical model of a DGD system and estimate its unknown parameters from field data.

Subtasks:

- Find a suitable model for the DGD system.
- Find sensitivities of parameters and determine how to find each of the parameters.
- Estimate unknown parameters which do not rely on dynamics.
- Estimate unknown parameters for a linearized version of the model.
- Estimate unknown parameters of the non-linear model.
- Possible augmentation of the model.

Preface

This report documents the work performed in connection with my Master's thesis during the spring semester of 2015. It completes the fifth and final year of my Master of Science program in Engineering Cybernetics at the Norwegian University of Science and Technology (NTNU).

The field of automated drilling technology is truly both fascinating and challenging. With the current trend in the oil and gas industry, it has never been more important to come up with solutions to improve efficiency as well as safety. To work with such important challenges as of today has been very motivational.

I would like to thank my supervisor at NTNU, Professor Ole Morten Aamo, for clarifying advice given during our frequent meetings. I would also like to thank Statoil ASA, represented by Espen Hauge and John-Morten Godhavn, for providing me the assignment together with the field data to be used for system identification. Thanks to Espen Hauge in particular for generously sharing his time throughout the semester. Our meetings provided much needed and appreciated inspiration for overcoming obstacles.

Trondheim, 2015

Dag Slettebø

Summary

Dual gradient drilling (DGD) is a modern technology that allows for drilling wells for oil and gas in a more precise and efficient manner. Many of the future oil and gas prospects are highly complex and challenging with narrow geo-pressure margins and little room for human errors. Such projects are simply only feasible if they are founded on robust and efficient automated drilling solutions that allow for accurate pressure control. This study focuses on investigation of a real DGD system in the Gulf of Mexico through modeling and application of field data in order to estimate unknown parameters.

First an introduction to the basics of drilling is given, explaining the advantages of the dual gradient drilling technology in terms of efficiency as well as safety. Then a hydraulic model for the complete system is developed. The available field measurements delimit a subsystem of the complete system where all parameters are identifiable. This shifts the focus of this thesis solely to the dynamics of the mud return line (MRL), which is the most vital section of the DGD system to know prior to control design.

Following the development of the model for the MRL dynamics, field data are applied to estimate the unknown parameters. Obvious discrepancies between observed field data and the outputs of the identified model expressions encourage slight modifications of the model structures until the observed outcomes are replicated by the model expressions to a satisfactory degree of accuracy. Finally, the dynamics of the identified system are simulated. The produced outputs are compared to field data, and the consistency between the simulation results and the field measurements works as a natural measure of the validity of the identified model.

Sammendrag

Dual gradient drilling (DGD) er en drillingteknologi som muliggjør drilling av brønner for olje og gass på en mer presis og effektiv måte. Mange av fremtidens olje- og gassprospekter er veldig komplekse i sin natur, med smale trykkmarginer og lite rom for menneskelige feil. Slike prospekter er simpelthen bare drillbare dersom de baseres på robuste og effektive løsninger som muliggjør presis kontroll av nedhullstrykket. Denne oppgaven har som fokus å undersøke et virkelig DGD-system i Mexicogulfen gjennom modellering og anvendelse av tilgjengelig feltdata for estimering av ukjente parametre.

Innledningsvis blir hovedprinsippene bak drilling forklart, med vekt på fordelene med DGD-teknologi hva angår effektivitet og sikkerhet. Deretter blir en hydraulisk modell for systemet utledet. De tilgjengelige feltmålingene avgrenser et subsystem av det fullstendige systemet hvor alle parametre er identifiserbare. Med dette skiftes fokuset i denne oppgaven til kun å omhandle dynamikken i returlinja (MRL), som er seksjonen av et DGD-system som det er mest vitalt at er kjent i forkant av kontrolldesign.

Etter at modellen for dynamikken i MRL er utledet kan feltdata bli anvendt til å estimere ukjente paremetre. Åpenbare avvik mellom de observerte feltdataene og utgangene fra de identifiserte modell-ligningene nødvendiggjør justering av modellstrukturene inntil de observerte målingene er replisert av ligningene i modellen med en tilfredstillende grad av nøyaktighet. Til slutt kan hele systemdynamikken simuleres, og de simulerte variablene kan sammenlignes med måledata. Graden av samsvar mellom simuleringsresultatene og feltmålingene fungerer som et naturlig mål på validiteten til den oppnådde systembeskrivelsen.

Table of Contents

List of Tables

List of Figures

Abbreviations

BOP	=	Blow Out Preventer
DGD	=	Dual Gradient Drilling
GoM	=	Gulf of Mexico
HPHT	=	High-Pressure, High-Temperature
LSE	=	Least Squares Estimate
MPD	=	Managed Pressure Drilling
MRL	=	Mud Return Line
NTNU	=	Norwegian University of Science and Technology
ODE	=	Ordinary Differential Equation
PDE	=	Partial Differential Equation
SPM	=	Subsea Pump Module

Chapter 1

Introduction

1.1 Background and Motivation

Drilling for petroleum hydrocarbons is carried out in vastly different environments worldwide, from the dry deserts of Saudi Arabia to the deep Gulf of Mexico. Deepwater drilling represents a particularly challenging business, as the pressure at such depths can be extraordinarily high. The fundamental nature of deepwater drilling operations - the search to discover volatile substances under extreme pressure in a hostile environment - inevitably implies some risk of fatal consequences, including loss of lives and massive spills to the environment. At the Macondo blowout and explosion accident on the Deep Water Horizon offshore drilling rig located in the Gulf of Mexico in April 2010, both of these consequences were brutally demonstrated. The accident resulted in the deaths of 11 workers, also leaving 17 seriously injured. The blowout also triggered the largest oil spill in US history with the estimated total discharge of 210 million US gallons of oil, resulting in severe damages to the close-by marine life.

In order to meet the continuing high demands for petroleum and energy worldwide, there is a great need to find new reserves and to extract these. Many of the larger fields that are accessible with conventional drilling technology have already been drilled. Consequently, many of the remaining fields typically contain less oil and gas, and are located in less accessible formations, making them harder to drill.

After the Macondo blowout accident, the industry has been stimulated to come up with new solutions improving safety. Also, as a result of fields becoming less accessible, the costs of drilling have increased significantly over the last few years. In the same time period, the oil price has dropped drastically, raising the threshold of investing in drilling operations. In order to enable drilling in a profitable as well as safe manner, it is therefore absolutely crucial that new and improved drilling technologies are developed.

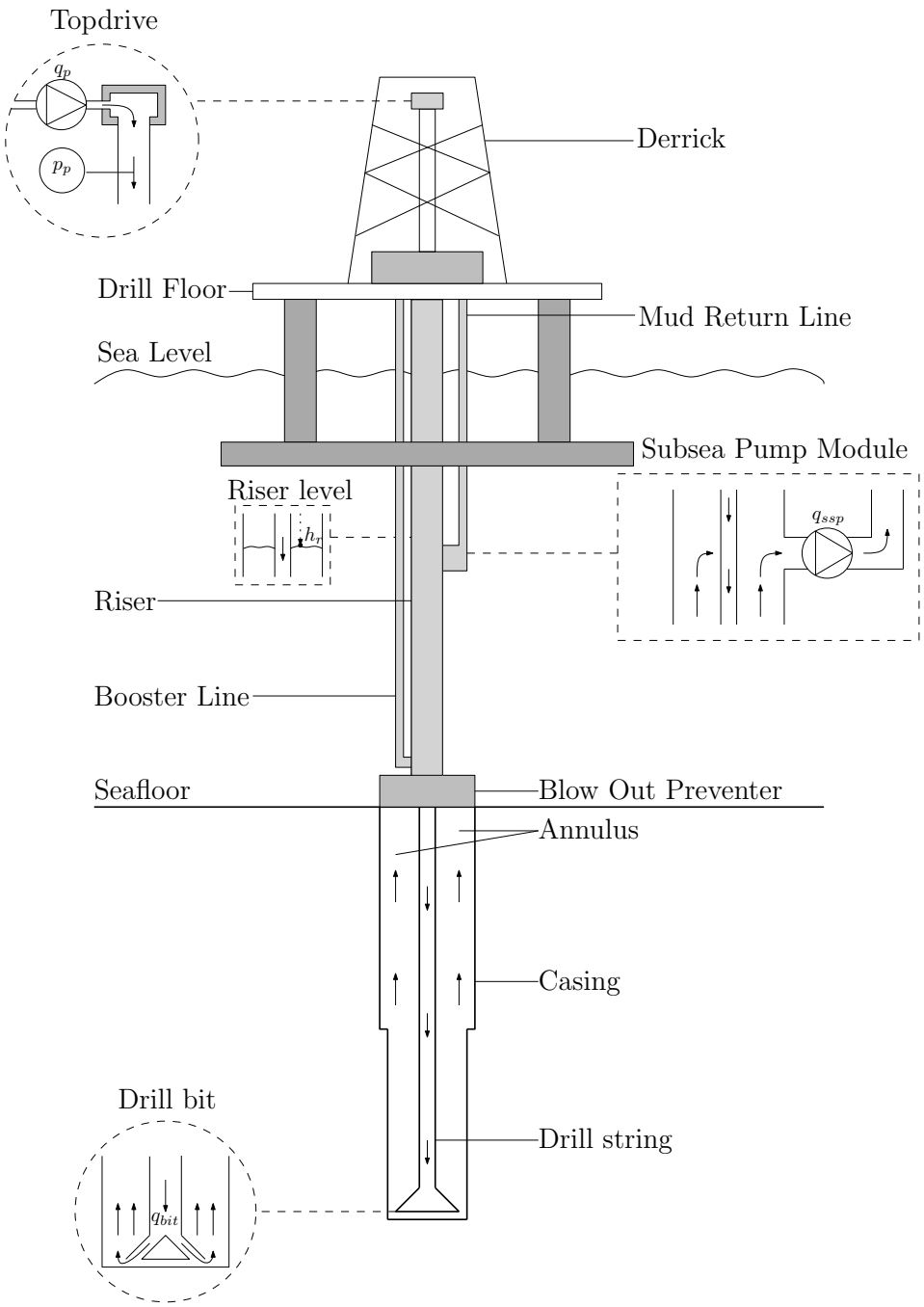

Figure 1.1: Offshore drilling from a semi-submersible drilling rig. The schematic is inspired by a similar figure from Stamnes [2011].

1.1.1 Mud circulation in a dual gradient drilling system

The basics of drilling can best be understood by considering the drill rig setup illustrated in Figure 1.1. The figure illustrates a semi-submersible platform performing offshore managed pressure drilling (MPD), in this case more precisely the variant known as dual gradient drilling (DGD). At the top of the derrick, the drill string is attached to the top drive motor, which is further attached to a hook, enabling the drill string to move up and down. As drilling progresses, the drill string sinks towards the drill floor, and after one length, a new stand of drill pipe is connected to the top before drilling can resume.

During any drilling operation, rock cuttings must be transported out of the wellhole. To serve this purpose, a circulation system based on a viscous fluid mixture called drilling mud is used. Mud from tanks on board the rig is fed to the main rig pump, which pumps the drilling mixture through the top drive and into the drill string. The mud continues down the drill string and out through the drill bit, which is located at the bottomhole of the well during regular operations. From this point, the flow of the viscous fluid collects and carries drill cuttings along up through the annulus and into the riser. In close vicinity to the blow out preventer (BOP), which is placed at seafloor level, an auxiliary line called the booster line, may provide supplementary injection of mud into the riser to assist in the circulation of drill cuttings when required. Even another mud flow, referred to as a topfill flow, may enter directly into the top of the riser, typically at a low constant flow rate. The purpose of the topfill is to break the surface of the mud column in the riser.

As opposed to in conventional drilling, the mud in a DGD system does not continue to flow up the riser all the way to the rig floor, but returns through a subsea pump and up a separate discharge line. This makes it possible to use the pump to control the level in the riser, which in turn affects the pressure profile in the annulus. This is a significantly faster and more convenient way to control pressure in the annulus than the tedious task of replacing the entire mud in the cycle with one of higher density, as is typically done in conventional drilling operations.

1.1.2 Drilling window and pressure control

The main reason for the need of pressure control is to maintain the annulus pressure profile within its margins, i.e. within the pressure zone that is often referred to as the drilling pressure window. The lower and the higher boundary of the window are represented by two of the most important parameters in designing and drilling a well for oil and gas, which are the well's pore pressure gradient and fracture pressure gradient, respectively.

Pore pressure is the pressure exerted by fluids within the pore space of formation rock, generated by the weight of the overburden rock and fluids above the formation. When a zone of porous hydrocarbon-bearing rock and sediment is encountered during drilling, the pore pressure will force oil and gas into the well unless the annulus pressure, generated by the weight of the mud column combined with friction due to mud flow, is high enough to counterbalance it. If the annulus pressure is below the pore pressure, then the well is

said to be under-balanced, and sections of the well may collapse and cause an influx of formation fluids into the wellbore from surrounding rock. Such an uncontrolled flow of hydrocarbons into a well is known in the industry as a kick. If a kick is not detected and controlled rapidly enough, it can cause an uncontrolled release of flammable oil and gas, commonly known as a blowout, whose potentially devastating consequences are known from the Macondo accident and several other similar occurrences. Even in cases where the kick is neutralized by proper handling, the kick could lead to undesirable consequences, e.q. a potential collapse of the well leading to a stuck drill string. In the worst case scenario, the pipe would need to be severed and parts of the well re-drilled. Ensuring that the pressure in the annulus is above the poor pressure is in other words absolutely essential to ensure safe as well as economically sound drilling operations.

The higher boundary of the drilling window is represented by the fracture pressure, which is the pressure that is required to fracture a rock formation. If the annulus pressure is above the fracture pressure, drilling mud will flow out of the wellbore and into the formation. This causes what is known as lost returns, lost circulation or simply a loss. A loss can damage the permeability of the reservoir . Also, the loss of fluid in one formation may be followed by the influx of fluid from another formation, potentially inducing a kick.

The pore and fracture pressure gradients are the measures of the respective pressure boundaries as a function of depth. Typically as a well is drilled deeper, the pore pressure and fracture gradients increase, but they don't always do so in tandem. This complicates a drilling operation. To maintain the integrity of the well at all times, it must be ensured that the mud column exerts pressure at the bottom of the well that is high enough to balance the pore pressure without exceeding the rock strength anywhere along an open section of the well. As the well is drilled deeper, the density of the mud required to balance the pore pressure will often eventually cause the pressure higher up in the wellbore to exceed the fracture pressure. The result is that drilling can not continue. As this happens, a casing in the form of a steel cylinder must be set into the well, enabling the drillers to increase the mud weight and continue operations without fracturing the shallower formations.

1.1.3 Advantages of dual gradient grilling

Deepwater drilling means higher hydrostatic pressure at the seabed, resulting in a more compact sediment formation. As a consequence, the pressure window is reduced. Such narrow drilling windows, also potentially caused by maturing of fields or depletion, often makes drilling prospects impractical to reach with conventional drilling methods, due to the lack of accurate control of the annular downhole pressure. In dual gradient drilling, the flexibility to adjust the annular pressure accurately by changing the riser level, makes it possible to keep the annular pressure very precise to fit tight drilling margins.

In conventional drilling, the pressure gradient of the mud itself always starts from the rig floor. This gradient often fits the drilling margins poorly, creating a need for frequent casing points and mud density changes, which result in a considerable amount of inefficient non-productive rig time. For dual gradient drilling, the flexibility in riser level adjustment

yields mud pressure gradients that starts at a lower depth, effectively moving the rig closer to the seafloor. A partially filled riser allows for the use of heavier mud weight, which improves cuttings transport and yields annular pressure gradients that fit the drilling window better, thus potentially improving casing the program and cementing operations. An illustrative comparison of the casing programs of dual gradient drilling versus conventional single gradient drilling is found e.g. in Fossum [2013].

1.1.4 Modeling of downhole pressure and control design

Due to harsh HPHT conditions at the bottomhole of a drilling well, accurate real-time measurements of the annular downhole pressure during drilling operations are most often unavailable. Thus, to gain accurate insight into the pressure conditions at the bottomhole of the well, a mathematical model of the hydraulic mud circulation system must be developed.

In order to control the pressure through feedback control algorithms, the model must also reflect the relationship between the subsea pump speed and the downhole pressure. This will allow the hydraulic model to output a subsea pump set-point associated with the desired downhole pressure as an input to a controller. Sufficient accuracy of the model is essential in order to ensure a safe and efficient automated dual gradient drilling operation.

After gaining operational experience with dual gradient drilling (DGD), field data has become available. This field data gives the opportunity to validate mathematical models and estimate unknown parameters. Once a verified model has been established, it can in turn be used to experiment with controller design and tuning. This will ease controller tuning offshore, which saves valuable rig time.

1.2 Previous Work

There exist a substantial amount of literature on MPD in general. A lot of effort has been put into developing advanced high fidelity models in order to capture all aspects of the drilling hydraulics, and multiple references to such literature are cited within Kaasa et al. [2011].

More specifically for DGD, a few simplified models are found e.g. in Breyholtz et al. [2009] and Breyholtz et al. [2011], where an existing model for MPD, produced in the mentioned Kaasa et al. [2011], is modified to fit the DGD system. Another simplified model that allows for multi-fluid dual gradient operations is found in Stamnes et al. [2012], where the complete model is made more realistic by including a model of the centrifugal subsea pump. Several other texts are also useful for understanding important and related concepts. In Landet [2011], a high order model for MPD system is presented based on discretizing the partial differential equations describing the hydraulic transmission line. Also, the work done by Anfinsen [2012] can be mentioned, where a low-order model for

simulation of the U-tube effect, caused by hydrostatic pressure difference between annulus and drill string, is developed.

1.3 Scope and Emphasis

A lot of effort has from the early 1990s until now been put into developing hydraulic models for MPD systems, both advanced high fidelity models and simpler, more transparent models. The DGD variant has been less investigated in papers due to the modern nature of the technology. The focus of this thesis will therefore to a great extent be directed towards modeling and system identification in connection to the dynamics of the mud return line, which is the section of the drilling system that is unique to DGD. However, this thesis still aims to provide a complete DGD system description.

The goal of the thesis is to identify and validate a mathematical model of the mud return line dynamics. Once a verified model has been established, it can serve as a necessary base to enable experimenting with controller design and tuning. Such experimenting will ease controller tuning offshore, which saves valuable rig time.

1.4 Structure of Thesis Report

This thesis report is organized as follows. Chapter 2 presents the complete modeling of the dual gradient drilling system. The chapter is introduced by reflection on the purpose of modeling, and proceeds with deriving generic low-order expressions for the pressure and flow dynamics of a flow section based on previous modeling work on MPD. Together with an expression for frictional pressure losses and a suggested model for the performance characteristics of the subsea pump, the generic equations for flow and pressure dynamics constitute the complete model of a DGD system. The chapter is rounded off by utilizing the found model to a real DGD system located in the Gulf of Mexico, whence field data are provided by Statoil ASA. Inspection of the amount of available measurements is used to determine what unknown parameters that can possibly be identified. In Chapter 3, appropriate system identification methods are utilized to estimate unknown system parameters. Corrections to the assumed model structures are suggested in cases where the identified models are unable to replicate the measured outcomes to a satisfactory degree. Chapter 4 completes the whole modeling and system identification process by simulation of the state equations of the model. The resulting state outputs are compared to the observed field data, functioning as a natural measure of the validity of the obtained system description. Chapter 5 summarized the results obtained in the thesis and presents a brief conclusion and final remarks.

Chapter 2

Modeling

A dual gradient drilling system shares many of the design characteristics with the original managed pressure drilling (MPD) system. The difference lies in the approach taken to manage and control the annular downhole pressure. The basic principle of MPD is to seal the top of the annulus and to control the mud flow from the well with a choke manifold in order to apply the desired back-pressure. A setup description of an automated MPD system is found e.g. in Riet et al. [2003]. A DGD system, on the other hand, consists of a separate mud return line and a subsea pump module (SPM) that allows for efficient control of the pressure profile in the annulus by regulating the mud level in the riser. Except for the end sections of the mud circulation systems, DGD and MPD systems are very similar, implying that much of the modeling from previous work on MPD systems can be equally applied to DGD systems.

2.1 Fit-For-Purpose Modeling

Prior to the establishment of a model of any real, physical system, it is useful to carefully consider ones objective of modeling, as it creates an awareness to work towards the most appropriate system description. The main goal of this thesis is to estimate unknown parameters needed in the mathematical system description. Secondly, in terms of control design, the model should reflect the relationship between the subsea pump speed and relevant states one might wish to control. This will allow for feedback control through real-time calculation of the subsea pump set point associated with the desired state reference.

Arguments in favor of a simpler, more transparent hydraulic model, to be used for downhole pressure estimation and control in MPD operations, are discussed in Kaasa et al. [2011]. This argumentation can be similarly applied in the context of the DGD system of this thesis, and is conveyed in the paragraphs to follow.

A high fidelity model to be used for detailed simulation and reproduction of a wide range of drilling-specific effects, necessarily requires a higher degree of complexity than a model to be used for control design. A system is inherently incapable of compensating for changes which are faster than a particular frequency range, known as the bandwidth of the closed-loop system. The bandwidth of the DGD system is typically determined by the dynamic response of the subsea pump, and the sampling rate of the control system. Therefore, it is undesirable that the output of the hydraulic model contains high-frequency dynamics.

With the main task of this thesis being system identification, the model should not be too advanced, since a complex model inevitably will make well-known parameter estimation schemes inadequate. Also, in many cases, the available measurements from field data contain insufficient information for identification of all parameters of an advanced model. Hence, without additional distributed measurements along the well, the sophisticated details of an advanced model may not contribute to improved accuracy in the system description and the control design.

Yet another argument that supports a simpler model, is the difficulty connected to rigorous verification of the numerical robustness of control algorithms that are based on complex models. The conditions in a well change during any drilling operation, meaning that parameters are both uncertain and slowly changing. Friction coefficients along the well are one example among others. To increase accuracy, the model should allow for calibration by application of algorithms for online parameter estimation. In an advanced model, the combination of complexity and a large number of unknown parameters, makes it hard to develop an online estimation scheme that allows for automatic calibration in a robust manner.

On the other hand, the model is in many cases the limiting factor for the achievable accuracy of the control system, and it is therefore crucial that the model captures the most dominant dynamics, in order for it to be an appropriate representation of the real world system and to achieve satisfactory control. Ideally, all together, the model should therefore be based on a suitable trade-off between accuracy and simplicity. Such a trade-off point can only be found through thorough analysis of the importance of the various dynamics in the specific system that is considered. Having this mindset within modeling is often referred to as *fit-for-purpose modeling*. Ways to remove unnecessary complexity are to neglect both very fast dynamic and very slow dynamics, and to lump together parameters which are not needed separately or are not possible to distinguish from one another in the available measurements.

Applying basic fluid dynamics to obtain a simple fit-for-purpose model will by necessity cause some lack of accuracy in the transient response. However, by incorporating accurate steady-state relations for the downhole pressure, the same steady-state accuracy can be achieved as with an advanced hydraulic model.

2.2 Assumption of a Viscous Drilling Fluid

Due to the many common properties of MPD and DGD systems, the hydraulic modeling assumptions of this section are similar to the general considerations around a simplistic model in Section 2.1, to a large extent based on the work done in the aforementioned MPD paper [Kaasa et al., 2011].

A main assumption that builds the foundation for the derivation of the hydraulic model is that the drilling fluid can be treated as a viscous fluid, which means that the flow is completely described by the following fundamental equations. The derivations are based on [Meritt, 1967] and [White, 1994].

- *Equation of state* The density as a function of pressure and temperature.
- *Fluid viscosity* The viscosity as a function of pressure and temperature.
- *Equation of continuity* The mass balance, or conservation of mass.
- *Equation of momentum* The force balance, or Newton's second law of motion.
- *Equation of energy* The energy balance, or the first law of thermodynamics.

The dynamics resulting from temperature effects reflected by the energy equation are outside the scope of this text and will be neglected in the modeling to follow. The effects of fluid viscosity will be discussed in relation to frictional losses in the flow, which is of relevance in the equation of momentum.

2.2.1 Equation of state

An equation of state provides a constitutive mathematical relationship between two or more state functions that is specific to a material or substance. The dependency of a matter's density of pressure and temperature can be written generally as

$$\rho = \rho(p, T) \tag{2.1}$$

where ρ, p and T denotes density, pressure and temperature, respectively.

This relationship is phenomenological, which means that it is not derived from physical fundamental principles, but found empirically through measured PVT[1] data which are interpolated. For a liquid, the changes in density are in general small, which makes it common to use the linearized equation of state around a reference point (ρ_0, p_0, T_0)

$$\rho = \rho_0 + \frac{\partial \rho}{\partial p}(p - p_0) + \frac{\partial \rho}{\partial T}(T - T_0) \tag{2.2}$$

[1] PVT = Pressure, Volume, Temperature.

By incorporating the material properties of the isothermal bulk modulus, β, and the isobaric cubical expansion coefficient, α, which are defined respectively as

$$\beta = \rho_0 \left(\frac{\partial p}{\partial \rho} \right)_T \tag{2.3a}$$

$$\alpha = -\frac{1}{\rho_0} \left(\frac{\partial \rho}{\partial T} \right)_p \tag{2.3b}$$

the linearized equation of state can be rewritten as

$$\rho = \rho_0 + \frac{\rho_0}{\beta}(p - p_0) - \rho_0 \alpha (T - T_0) \tag{2.4}$$

or in its differential form

$$d\rho = \frac{\rho}{\beta} dp - \rho \alpha dT \tag{2.5}$$

The accuracy of the linearization will always decrease with increasing pressure and temperatures, but it has been shown to be fairly accurate for most drilling fluids in the ranges $0 - 500\,\mathrm{bar}$ and $0 - 200\,^\circ\mathrm{C}$, which can be verified by PVT data e.g. in Isambourg et al. [1996].

Even though significant temperature gradients may exist in a drilling system, in particular for HPHT wells, the thermal expansion coefficient α for liquids is usually small, which is an argument to neglect density changes as a function of temperature changes. Also, compared to pressure transients, which are in range of seconds and minutes, temperature transients are in range of minutes and hours. The slow pressure effects that may be caused by temperature changes can usually be handled more efficiently by online calibration based on feedback in the control system, than to include these effects in the model as dynamics. Neglecting the dependence of temperature yields the following equation of state for the density dynamics

$$d\rho = \frac{\rho}{\beta} dp \tag{2.6}$$

2.2.2 Equation of continuity

The equation of continuity of mass states that the rate at which mass enters a system volume equals the rate at which it leaves the volume + the rate at which mass accumulates in the volume due to compressibility effects. In the modeling of the mud flow, is is reasonable to assume that the flow is radially homogeneous and that it can be treated as one-dimensional along the main flow path. For 1-D flow, the differential mass continuity equation can be written

$$\frac{\partial \rho}{\partial t} + \frac{\partial}{\partial x}(\rho \nu) = 0 \tag{2.7}$$

where ν is the velocity of the flow, and x is the spatial variable along the flow path. The expression for the density time derivative as given by Eq. 2.7 can be substituted into the

expression for the pressure time derivative in Eq. 2.6 to yield an expression for the pressure dynamics as a function of flow velocity

$$\frac{\partial p}{\partial t} = \frac{\beta}{\rho}\frac{\partial \rho}{\partial t} = -\frac{\beta}{\rho}\frac{\partial}{\partial x}(\rho\nu) = -\frac{\beta}{\rho}\left(\frac{\partial \rho}{\partial x}\nu + \frac{\partial \nu}{\partial x}\rho\right) \tag{2.8}$$

By assuming that the flow is spatially incompressible, i.e. $\frac{\partial \rho}{\partial x} \approx 0$, and that the cross-sectional area $A(x)$ is close to piecewise constant, the expression in Eq. 2.8 can be simplified to

$$\frac{\partial p}{\partial t} = -\beta\frac{\partial \nu}{\partial x} = -\beta\frac{\partial\left(\frac{q}{A(x)}\right)}{\partial x} = -\frac{\beta}{A}\frac{\partial q}{\partial x} \tag{2.9}$$

where q denotes the volume flow rate.

The expression for the pressure dynamics found in Eq. 2.9 is the same as that is found from derivation of the model for a hydraulic transmission line in Egeland and Gravdahl [2002], linearized around zero flow ($q = 0$) and atmospheric pressure ρ_0. It is reproduced below exactly as stated in the reference text, with explicit dependence on time and spatial position

$$\frac{\partial p(x,t)}{\partial t} = -\frac{\beta}{A}\frac{\partial q(x,t)}{\partial x} \tag{2.10}$$

The main compressibility effects accounted for in Eq. 2.6 - 2.7 through the bulk modulus β, characterizes the dominating dynamics of the hydraulic system, and is reflected in the pressure along the entire flow path. The pressure dynamics at any point can therefore be approximated quite accurately by the dynamics of the average pressure in the entire well, offset with the hydrostatic pressure and friction drop relative to a fixed reference point. Integration of mass flow over a control volume yields the integral form of the continuity equation in Eq. 2.7

$$\frac{d}{dt}(\rho V) = \rho\frac{dV}{dt} + V\frac{d\rho}{dt} = \rho_{in}q_{in} - \rho_{out}q_{out} \tag{2.11}$$

where V is the control volume, ρ is the average density and $\rho_{in}q_{in}$ and $\rho_{out}q_{out}$ are the the mass flow rates in and out of the control volume, respectively. Substituting for the density dynamics derived in Eq. 2.6 yields the control volume pressure dynamics

$$V\frac{d\rho}{dt} = V\frac{\rho}{\beta}\frac{dp}{dt} = -\rho\frac{dV}{dt} + \rho_{in}q_{in} - \rho_{out}q_{out} \tag{2.12}$$

With the assumption of spatially homogeneous density, i.e. that the density in and out of the control volume equal the average density, $\rho_{in} = \rho_{out} = \rho$, the pressure dynamics expression in Eq. 2.12 is further simplified to

$$\frac{V}{\beta}\frac{dp}{dt} = -\dot{V} + q_{in} - q_{out} \tag{2.13}$$

It is not hard to see that given a constant density within the control volume, the control volume approach corresponds to approximating the spatial derivative of the flow rate through a certain flow section from the advanced model of Eq. 2.10 by

$$\frac{\partial q}{\partial x} \approx \frac{q_{out} - q_{in} + \dot{V}}{\Delta x} \tag{2.14}$$

as indicated by the control volume figure in Fig. 2.1. With this approximation substituted into the advanced model of Eq. 2.10, the same expression for the average pressure dynamics as in Eq. 2.13 is obtained as expected:

$$\dot{p} = -\frac{\beta}{V}(q_{out} - q_{in} + \dot{V}) \tag{2.15}$$

where the control volume $V = A\Delta x$ has been defined.

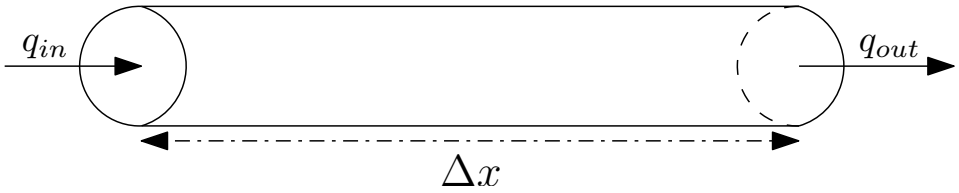

Figure 2.1: A control volume for the discretization of pressure dynamics in a hydraulic transmission line.

2.2.3 Equation of momentum

A force balance based on conservation of momentum is developed in White [1994] for one-dimensional time invariant density and viscosity. Density effects in the flow have been shown only to become significant as the flow approaches the speed of sound. The flow is generally termed incompressible for Mach number less than 0.3. The resulting PDE, with flow rate q as main variable, based on the assumption of piecewise constant cross-sectional area $A(x)$, is written as

$$\frac{\rho}{A}\frac{dq}{dt} = -\frac{\partial p}{\partial x} - \frac{\partial \tau}{\partial x} + \rho g \cos(\theta(x)) \tag{2.16}$$

where q denotes volume flow rate, ρ denotes mud density, p denotes pressure, g denotes the gravitational constant, τ denotes viscous frictional force per spatial unit and $\theta(x)$ denotes the slope of the flow path at location x.

The friction term τ is typically a lumped friction term depending on the velocity of the flow, and is constituted of frictional losses due to viscous dissipation, turbulence, swirl flow and non-ideal flow conditions (section changes, bends, etc.), often referred to as *minor losses*.

Pressure transients propagate as pressure waves in the mud at the speed of sound, which is given by the Newton-Laplace equation as the square root of the ratio between fluid

stiffness (bulk modulus) and fluid density:

$$c = \sqrt{\frac{\beta}{\rho}} \tag{2.17}$$

However, the speed of sound is typically high for a hydraulic oil, resulting in very fast pressure propagation dynamics. These high-frequency dynamics are typically much faster than the bandwidth of the control system, and it is therefore reasonable to neglect them.

Similar to the case for the pressure dynamics, the PDE describing the flow dynamics in Eq. 2.16 can be approximated by an ODE by applying simplifying assumptions. Assuming that the fluid accelerates homogeneously as a stiff mass, i.e. $\frac{\partial q}{\partial x} \approx 0$, Eq. 2.16 can be integrated along the flow path to give an equation for the average flow rate dynamics.

$$M(l_1, l_2)\dot{q} = p_1 - p_2 - F(l_1, l_2, q, \mu) + G(l_1, l_2, \rho) \tag{2.18}$$

where

$$M(l_1, l_2) = \int_{l_1}^{l_2} \frac{\rho(x)}{A(x)} dx \tag{2.19a}$$

$$F(l_1, l_2, q, \mu) = \int_{l_1}^{l_2} \frac{\partial \tau(q/A(x), \mu)}{\partial x} dx \tag{2.19b}$$

$$G(l_1, l_2, \rho) = \int_{l_1}^{l_2} \rho(x) g \cos(\theta(x)) dx \tag{2.19c}$$

Here, q is the average flow rate between $x = l_1$ and $x = l_2$, p_1 and p_2 denote pressure respectively at $x = l_1$ and $x = l_2$, $M(l_1, l_2)$ is the density per cross-section integrated over the flow path, $F(l_1, l_2, q, \mu)$ is the integrated frictional losses along the flow path and $G(l_1, l_2, \rho)$ is the total gravity affecting the fluid.

2.3 Frictional Pressure Losses

The friction term in Eq. 2.19b must be given particular attention, as detailed modeling of frictional losses represents a significant challenge, even in the presence of extensive system knowledge. In general, drilling fluids are non-Newtonian, which implies that their viscosity depends on shear rate or shear rate history. Considering these non-Newtonian properties of the drilling mud complicates friction calculations, and is outside the scope of this thesis. Hence the mud will be assumed Newtonian in the following work. As stated in Kaasa et al. [2011], the viscosity of a liquid decreases markedly with temperature, and increases somewhat with pressure, and may in general be written as

$$\mu = \mu(p, T) \tag{2.20}$$

Typically, the dependence on pressure is negligible. Furthermore, since temperature dynamics are outside the scope of this text, the viscosity will be assumed constant in the following friction modeling.

The flow path will normally contain both laminar and turbulent flow regimes as well as transitions between these regimes. To find an expression for the pressure losses along any flow path, a generic method that distinguishes between laminar and turbulent flow regimes can be used. To determine whether the flow at a given location l is laminar or turbulent, the Reynolds number is calculated as

$$Re(l) = \frac{4\rho}{\pi d(l)\mu} q \tag{2.21}$$

where $d(l)$ is the cross-sectional diameter at location l and the other variables denote measures as previously described. If the Reynolds number is below $Re_{crit} = 2300$, the flow is deemed to be laminar. Otherwise it is turbulent. To obtain the pressure loss in the interval $[l_0, l_1]$, the phenomenological Darcy-Weisbach equation is used

$$F(q) = \int_{l_0}^{l_1} f(l) \frac{8\rho}{\pi^2 d(l)^5} q^2 dl \tag{2.22}$$

where the friction factor is given by

$$f(l) = \frac{64}{Re(l)} \tag{2.23}$$

for laminar flow, and

$$f(l) = \left(-1.8 \log \left[\frac{6.9}{Re(l)} + \left(\frac{\epsilon}{3.7 d(l)} \right)^{1.11} \right] \right)^{-2} \tag{2.24}$$

for turbulent flow, where ϵ is the measure of the wall roughness, see e.g. [White, 1994].

In addition to frictional pressure losses along flow paths, considerable losses of variable degree also exist in various equipment in a typical dual gradient drilling setup, including topside equipment and drill bit assembly. An expression for the frictional losses over a drill bit assembly is suggested in Stamnes et al. [2012] as

$$F_{bit} = \frac{\rho_d(l_{bit}) q^2}{2 C_v^2 TFA^2} \tag{2.25}$$

where C_v denotes the discharge coefficient and TFA denotes the total fluid area in the bit [API, 2006].

In a situation where no information exists about system parameters like the wall roughness ϵ and/or the mud viscosity μ, the unknown parameters must be estimated before the Darcy-Weisbach can be used to model the frictional losses along flow sections. Estimation of these parameters is cumbersome due to the intricate nonlinear nature of the friction factor expression in Eq. 2.24. Furthermore, parameter information needed in determining the

friction characteristics of equipment that potentially cause significant pressure losses, can typically also be difficult to obtain, as exemplified by the unknown parameters in Eq. 2.25. A possible approach to obtain a structurally simpler model is to approximate the original partially unknown function for the frictional pressure losses by its Taylor series. By assuming that the frictional losses can be approximated as the second order Taylor polynomial evaluated around zero flow, also called a Maclaurin series, the expression becomes

$$F(q) = C \cdot q + D \cdot q^2 \tag{2.26}$$

which is linear in its unknown parameters C and D. The physical interpretation of the polynomial coefficients are abstracted away in such a model. On the positive side, due to its simple structure, parameter estimation becomes straightforward, granted that observed data measurements of flow rate and pressure losses are available.

2.4 Subsea Pump Module

The centrifugal subsea pump that lifts the fluid from the riser and up to the rig is modeled as a dynamic pump as opposed to a positive displacement pump. This implies that the flow rate through the pump, q_{ssp}, depends not only on the pump rotation speed, ω_{ssp}, but also on the operational point where the pressure required to move fluid through the system equals the available pressure produced by the pump.

In the fluid mechanics literature, e.g. [Çengel and Cimbala, 2010], the measure of *net head* is often used instead of pressure in the context of pump performance. The available net head or pump head H, is defined as the change in *Bernoulli head* between the inlet and outlet of the pump. Net head has the dimension of length, calculated as the equivalent column height of fluid that would generate a given pressure. For the case of incompressible flow through a liquid pump in which the inlet and outlet diameters are identical, and there is no change in elevation, the expression for the available net head is given as

$$H = \frac{P_{out} - P_{in}}{\rho g} \tag{2.27}$$

For this case, the pump head is simply the pressure rise across the pump divided by gravitational acceleration and the density of the fluid. This fluid is often assumed to be water, even for a pump that is not pumping water. In this thesis, however, head will be defined as the equivalent column height of mud, corresponding to defining $\rho = \rho_{mud}$ in Eq. 2.27. Since the flow itself has been assumed incompressible in the previous modeling sections, it is convenient to use this definition of pump head throughout the thesis.

The maximum flow rate through a pump occurs when the pump head is zero. This flow rate is referred to as the pump's *free delivery*, and this condition is achieved when there is no load on the pump. At the other extreme, the *shutoff head* is the pump head that occurs when the volume flow rate is zero, and is achieved when the outlet is blocked. During regular operations, the actual flow rate will always stay between these two extremes. The

pump head may increase from its shutoff value somewhat as the flow rate increases, but the head must by necessity eventually decrease to zero as the volume flow rate increases to its free delivery. Curves of the available pump head as a function of flow rate are called *pump performance curves* or *characteristics curves*. Since the pump head increases with rotational speed, a specific pump curve exists for each corresponding pump speed.

The pump head expression for a particular pump is typically found through experimental testing. In Stamnes et al. [2012], it is argued that it is not hard to approximate the pump head model using the so called affinity laws, described e.g. in White [1994]. The suggested model used is

$$\Delta H_{SPM}(\omega_{ssp}, q_{ssp}) = c_0\omega_{ssp}^2 - c_1\omega_{ssp}q_{ssp} - c_2 q_{ssp}^2 \tag{2.28}$$

where c_0, c_1 and c_2 are fitting constants for each individual pump. With all coefficients positive, the pump curve becomes strictly decreasing with increased flow.

2.5 Simplified Hydraulic Model of Complete Dual Gradient System

To summarize, the following relevant models have been derived:

- Section 2.2: Pressure and flow rate dynamics of mud based on the viscous fluid assumption.
- Section 2.3: Frictional pressure losses as function of flow rate
- Section 2.4: Characterization of the subsea pump head as a function of rotational speed and flow rate.

Incorporation of the found models with the mud circulation structure of a DGD system described in Subsection 1.1.1 form the foundation for a complete hydraulic model description. The model can be roughly divided into pressure dynamics and flow rate dynamics for each of the various drill system sections: drill string, booster line, annulus and mud return line.

2.5.1 Pressure dynamics

The drill string and the booster line are pressurized and closed from the atmosphere, which makes it reasonable to take compressibility into account for these sections. The annulus and the return line, on the other hand, are open to atmosphere, which justifies neglecting the compressibility effects caused by pressure variations for these sections.

Drill string

The drill string can be modeled as a hydraulic system with a single fluid. Since the drill string volume is constant during drilling, total volume changes can be neglected, yielding $\dot{V}_d = 0$. Based on the discretized hydraulic model in Eq. 2.15, using the whole drill string as a single control volume, the pressure dynamics can be written as

$$\frac{V_d}{\beta_d}\dot{p}_p = q_p - q_{bit} \tag{2.29}$$

where p_p denotes mud pump pressure, q_p denotes volume flow rate through the rig pump, q_{bit} denotes volume flow rate through the drill bit, V_d denotes drill string inner volume and β_d denotes the isothermal bulk modulus of the mud.

Booster line

The booster line pressure dynamics can be modeled similarly to the drill string pressure dynamics, giving

$$\frac{V_b}{\beta_b}\dot{p}_b = q_{bp} - q_{boostIn} \tag{2.30}$$

where p_b denotes booster pump pressure, q_{bp} denotes volume flow rate through the booster pump, $q_{boostIn}$ denotes volume flow rate into the annulus , V_b denotes booster line inner volume and β_b denotes the isothermal bulk modulus of the mud.

Annulus

The riser is open to atmospheric pressure, which justifies neglecting the compressibility of the mud in this section. The assumption thus reduces the mass balance into a volume balance for the total volume of fluid in the annulus, giving

$$\dot{V}_a = q_{bit} + q_{boostIn} + q_{tf} - q_{ssp} \tag{2.31}$$

where q_{bit} is the flow entering the annulus through the drill bit, $q_{boostIn}$ is the inflow from the booster line, q_{tf} is the top fill rate and q_{ssp} is the outflow through the subsea pump.

The riser level, h_r, indicating how much of the annulus that is not filled with mud, defined with positive sign in the downwards direction, changes in the opposite direction of the annulus mud volume and satisfies

$$\dot{h}_r = \frac{q_{ssp} - (q_{bit} + q_{boostIn} + q_{tf})}{A_a(h_r)} \tag{2.32}$$

where $A_a(h_r)$ is the cross-sectional area of the annulus at location h_r.

Mud return line

The mud return line is open to atmospheric pressure as the annulus, justifying negligence of the compressibility effects. Furthermore, the MRL is assumed to be constantly filled

with mud, meaning that the level does not change. This assumption further implies that the flow into the MRL through the subsea pump, q_{ssp}, equals the flow out of the return line at the rig, q_{MRL}, which can be described with the trivial equation

$$\dot{V}_{MRL} = q_{ssp} - q_{MRL} = 0 \tag{2.33}$$

2.5.2 Flow rate dynamics

Drill string

The dynamics of the flow through the drill bit can be assumed approximately equal to the dynamics of the average flow that originates from the mud pump and ends up at the inlet of the MRL. Applying the model for the average flow dynamics found in Eq. 2.18 - 2.19 gives the expression for the drill bit flow dynamics

$$M_d(h_r)\dot{q}_{bit} = p_p - p_0 - [F_d(q_{bit}) + F_a(h_r, q_{bit} + q_{boostIn})] + \Delta G_d(h_r) \tag{2.34}$$

where

$$M_d(h_r) = \int_0^{l_{bit}} \frac{\rho(x)}{A_d(x)} dx + \int_{h_r}^{l_{bit}} \frac{\rho(x)}{A_a(x)} dx \tag{2.35}$$

Here, p_p is the mud pump pressure, p_0 is the atmospheric pressure (at the riser level h_r), l_{bit} is the length of the drill string and in this case the same as the true vertical depth of the drill bit, $F_d + F_a$ are the total steady-state frictional pressure losses in the drill string and the annulus combined, calculated as described in Section 2.3, and ΔG_d is the hydrostatic steady-state pressure difference between the drill string and the annulus. Both the drill string and the annulus are assumed to be straightly vertical, which yields the straightforward expression

$$\Delta G_d(h_r) = \rho g l_{bit} - \rho g(l_{bit} - h_r) = \rho g h_r \tag{2.36}$$

With the assumption of constant drill string and annulus cross-sectional areas, the expression for the integrated density per cross-section in Eq. 2.35 can be written directly as

$$M_d(h_r) = \frac{\rho \cdot l_{bit}}{A_d} + \frac{\rho \cdot (l_{bit} - h_r)}{A_a} \tag{2.37}$$

Booster line

An almost identical expression for the flow in from the booster line can be stated as for the drill string

$$M_b(h_r)\dot{q}_{boostIn} = p_b - p_0 - [F_b(q_{boostIn}) + F_a(h_r, q_{bit} + q_{boostIn})] + \Delta G_b(h_r) \tag{2.38}$$

where

$$M_b(h_r) = \int_0^{l_{boost}} \frac{\rho(x)}{A_b(x)} dx + \int_{h_r}^{l_{boost}} \frac{\rho(x)}{A_a(x)} dx \tag{2.39}$$

Here, p_b is the booster pump pressure, p_0 is the atmospheric pressure (at the riser level h_r), l_{boost} is the length of the booster line and the same as the true vertical depth of the booster inlet, $F_b + F_a$ are the total steady-state frictional pressure losses in the booster line and the annulus combined, calculated as described in Section 2.3, and ΔG_b is the hydrostatic steady-state pressure difference between the booster line inlet and the annulus

$$\Delta G_b(h_r) = \rho g l_{boost} - \rho g(l_{boost} - h_r) = \rho g h_r \tag{2.40}$$

The expression in Eq. 2.39 is similar to Eq. 2.35 simplified to yield a straightforward expression

$$M_b(h_r) = \frac{\rho \cdot l_{boost}}{A_b} + \frac{\rho \cdot (l_{boost} - h_r)}{A_a} \tag{2.41}$$

Mud return line

The flow rate through the subsea pump was assumed equal to the flow out from the MRL as given by Eq. 2.33, and its dynamics can also be described by the model for average flow dynamics in the MRL as described by Eq. 2.18 - 2.19, giving

$$M_{MRL}(h_r)\dot{q}_{ssp} = P_{SPM_{IN}}(h_r) + \Delta P_{SPM}(\omega_{ssp}, q_{ssp}) - p_0 - F_{MRL}(q_{ssp}) - G_{MRL} \tag{2.42}$$

where

$$M_{MRL}(h_r) = \int_{h_r}^{h_{SPM_{IN}}} \frac{\rho(x)}{A_a(x)} dx + \int_0^{h_{SPM_{OUT}}} \frac{\rho(x)}{A_{MRL}(x)} dx \tag{2.43}$$

Here, $P_{SPM_{IN}}(h_r)$ is the pressure at the SPM inlet. The frictional losses from the riser level to the SPM inlet are neglected due to the unclear flow conditions of this section, giving the SPM inlet pressure purely as a function of riser level,

$$P_{SPM_{IN}}(h_r) = p_0 + \rho g(h_{SPM_{IN}} - h_r) \tag{2.44}$$

ΔP_{SPM} is the pressure rise produced by the subsea pump, calculated from the pump head expression in Eq. 2.28, $h_{SPM_{IN}}$ and $h_{SPM_{OUT}}$ are the depth elevation respectively of the subsea pump inlet and outlet, p_0 is the atmospheric pressure (at the MRL outlet), F_{MRL} is the total steady-state frictional pressure losses in the mud return line, calculated as described in Section 2.3, and G_{MRL} is the constant hydrostatic steady-state pressure generated by the volume of fluid in the assumed to be constant filled mud return line

$$G_{MRL} = \rho g h_{SPM_{OUT}} \tag{2.45}$$

With the assumption of constant annulus and return line cross-sectional areas, the expression for the integrated density per cross-section in Eq. 2.43 can be written directly as

$$M_{MRL} = \frac{\rho \cdot (h_{SPM_{IN}} - h_r)}{A_a} + \frac{\rho \cdot h_{SPM_{OUT}}}{A_{MRL}} \tag{2.46}$$

2.5.3 State-space representation

The dynamical model for the complete system can be written as a state-space representation by collecting the expressions for the pressure and flow dynamics in all sections of the DGD system. The dependence on variables of various expressions are written out here for clarity, giving:

$$\dot{p}_p = \frac{\beta_d}{V_d}(q_p - q_{bit}) \tag{2.47a}$$

$$\dot{p}_b = \frac{\beta_b}{V_b}(q_{bp} - q_{boostIn}) \tag{2.47b}$$

$$\dot{h}_r = \frac{q_{ssp} - (q_{bit} + q_{boostIn} + q_{tf})}{A_a(h_r)} \tag{2.47c}$$

$$\dot{q}_{bit} = \frac{1}{M_d(h_r)}(p_p - p_0 - [F_d(q_{bit}) + F_a(h_r, q_{bit} + q_{boostIn})] + \Delta G_d(h_r)) \tag{2.47d}$$

$$\dot{q}_{boostIn} = \frac{1}{M_b(h_r)}(p_b - p_0 - [F_b(q_{boostIn}) + F_a(h_r, q_{bit} + q_{boostIn})] + \Delta G_b(h_r)) \tag{2.47e}$$

$$\dot{q}_{ssp} = \frac{1}{M_{MRL}(h_r)}(P_{SPM_{IN}}(h_r) + \Delta P_{SPM}(\omega_{ssp}, q_{ssp}) - p_0 - F_{MRL}(q_{ssp}) - G_{MRL}) \tag{2.47f}$$

The system in Eq. 2.47 is nonlinear with $p = 4$ typical input variables to the system $(q_p, q_{bp}, q_{tf}, \omega_{ssp})$ and $n = 6$ state variables, and is solvable for given initial conditions provided that all unknown parameters are estimated.

2.6 Drilling Setup and Statoil Field Data

The purpose of the model in Eq. 2.47 is to function as a representation of the dominating dynamics of a real DGD system. After gaining operational experience with dual gradient drilling, field data from such drilling facilities have become available. The data of this thesis are provided by Statoil ASA, recorded in the time interval 7th - 10th of October 2014 from drilling operations at an unspecified drilling rig in the Gulf of Mexico.

The raw field data were handed over in the MAT-file format for easy loading into the workspace of MATLAB, and include flow and pressure measurements at various sections of the drilling system, in addition to subsea pump speed set-points. The dynamic response of the pump is claimed to be very quick. The engine is large, and the frequency converter is assumed to ensure that the pump speed converges to its reference in a negligible short transient period. Therefore, the set-point of the pump is applied as a pump speed measurement for the rest of this thesis.

Most data were recorded at a sampling frequency of 1 Hz. Pressure measurements at the inlet and the outlet of the SPM are found through averaging two redundant measurements to reduce potential measurement and calibration errors. A schematic of the Gulf of Mexico DGD system with the measurement transmitters at their respective locations is shown in Fig. 2.2. The locations of the state variables of Eq. 2.47a - 2.47f are indicated as black circle marks together with the associated equation letter, and the corresponding state names are listed in the text box. The available transmitters and the names and units of their associated measurements are listed in Table 2.1. A list of priorly known system parameters are given in Table 2.2.

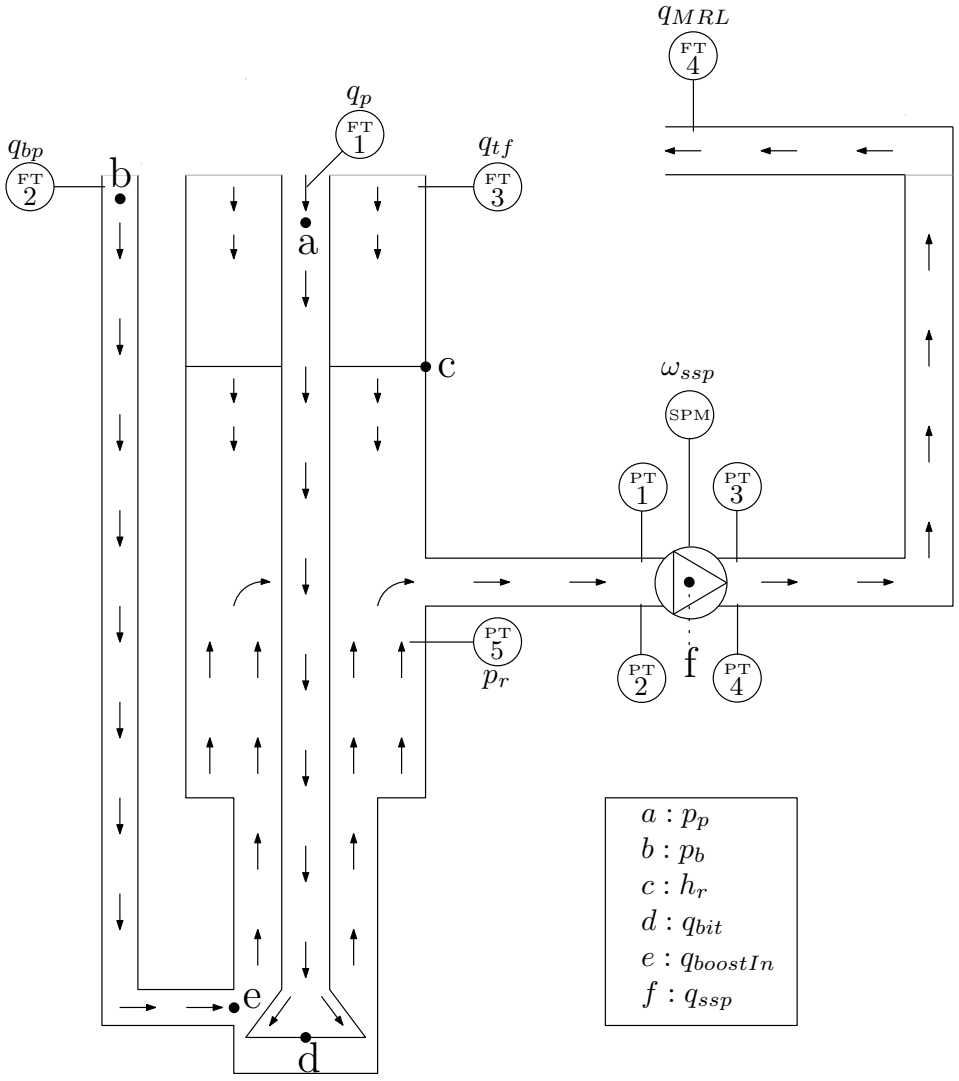

Figure 2.2: Schematic of the GoM Dual Gradient Drilling system.

Table 2.1: DGD measurements from GoM provided by Statoil.

Transmitter	Variable name	Unit	Description
FT 1	q_p	gpm	Mud pump flow
FT 2	q_{bp}	gpm	Booster pump flow
FT 3	q_{tf}	gpm	Top fill flow
FT 4	q_{MRL}	gpm	Return flow
PT 1	$P_{SPM_{IN,1}}$	psi	SPM Inlet pressure 1
PT 2	$P_{SPM_{IN,2}}$	psi	SPM Inlet pressure 2
PT 3	$P_{SPM_{OUT,1}}$	psi	SPM Outlet pressure 1
PT 4	$P_{SPM_{OUT,2}}$	psi	SPM Outlet pressure 2
PT 5	p_r	psi	Riser pressure
SPM	ω_{ssp}	$\%(0-100)$	Subsea pump speed (reference)

Table 2.2: List of known parameters of GoM DGD well.

Description	Variable name	Size	Unit
Mud weight	ρ	1.08	sg[2]
Riser ID	riserID	19.5	inch
Drillpipe OD	drillpipeOD	6.625	inch
Casing OD	casingOD	$13\frac{5}{8}$	inch
Mud return line ID	mrlID	6	inch
Booster line ID	boosterID	4	inch
Inlet to SPM	hSPMin	350.30	mRKB[3]
Outlet of SPM	hSPMout	350.30	mRKB
Riser pressure sensor	hPRiser	352.10	mRKB
Booster line inlet	boosterInlet	1494	mRKB
Wellhead Datum	wellheadDatum	1510	mRKB

The flow rate and pressure variables of Table 2.1 are originally given in typical U.S. units, namely gpm (US gallon per minute) and $\mathrm{psi(a)}$ (Pounds per square inch absolute). Also, the diameters of Table 2.2 are given in the US length unit inch. For simplicity, all measurements and parameters are converted into their SI unit counterparts, namely m^3/s for flow rate, Pa for pressure and m for diameters, before they are used in calculations. The conversion factors from US units to their respective SI units are given in Table 2.3.

[2]Specific gravity (ratio of density of mud to density of water).
[3]Depth in meters relative to kelly bushing.

Table 2.3: Conversion factors from US to SI units.

US unit	SI unit	Conversion factor
gpm	m^3/s	$6.3090 \cdot 10^{-5}$
psi	Pa	6894.75729
inch	m	0.0254

2.7 System Identification Feasibility

The state-space model for the complete GoM dual gradient drilling system in Eq. 2.47 can earliest be used in simulation of the dynamics when all unknown parameters are identified. However, in order to apply estimation methods to a given equation containing unknown parameters, all variables included must be available as recorded field measurements, or at least as good approximations. The subset of the states of the system in Eq. 2.47 that can be simulated, therefore depends on what parameters that can be estimated from the available field data from the GoM well.

The field data provide little information about the pressure conditions in vicinity of the mud pump and the booster pump. Due to the fact that no knowledge is possessed of the actual pressure measurements from periods when field data were collected, the isothermal bulk modulus of the mud cannot be estimated from measurements in any direct way. Hence, simulation of the pressure dynamics in the drill string and the booster line described by Eq. 2.47a - 2.47b will be difficult. This further has consequences for the possibilities to simulate the flow dynamics out from the drill bit and at the booster inlet, since, without pump pressure and booster pump pressure as available states or input variables, Eq. 2.47d - 2.47e are also incomplete.

The terms of frictional pressure losses in the latter two equations are also highly uncertain. Parameters like the mud viscosity and wall roughness needed to calculate frictional losses from the Darcy-Weisbach equation in Eq. 2.22 for a given flow rate, are not listed in Table 2.2. A prerequisite of applying the model is therefore that its unknown parameters are identifiable. However, there are neither nearby pressure measurements nor flow rate measurements to base estimates on. A model of the frictional losses will therefore be hard to obtain both in the drill string, booster line and the annulus.

The riser level derivative h_r in Eq. 2.47c is a function of the unavailable flow rate states, q_{bit} and $q_{boostIn}$. However, assuming that the fluid accelerates close to homogeneously as a stiff mass in the drill string and the booster line, the unavailable flow rates can be approximated by their available input counterparts, q_p and q_{bp}, respectively. Adjustments in the form of time delay terms to correct for unmodeled dynamics may later be proven necessary to obtain sufficient accuracy. The topfill rate q_{tf} is known from measurements, and the cross-sectional area of the annulus is known from the diameter given in Table 2.2, which is constant at all depths. Therefore, all information needed to simulate the riser level dynamics is available.

The variables of the equation for the flow rate dynamics through the subsea pump in Eq. 2.47f are either seemingly available states (h_r, q_{ssp}) or the available input ω_{ssp}. All unknown parameters are included in expressions that convey some relationship between the MRL flow rate, subsea pump speed and some pressure measurement within the MRL. As seen from the system setup schematic in Figure 2.2, both pressure, flow rate and pump speed measurements are available in the MRL, making system identification of unknown parameters likely feasible. With estimated unknowns available, it is possible to calculate the subsea flow rate derivative, so that the system in Eq. 2.47f can be simulated.

2.8 Hydraulic Model of Mud Return Line for System Identification

The reasoning in Section 2.7 makes it clear that the remaining candidates of state equations feasible for parameter identification and simulation are those affiliated with the MRL section, namely the riser level dynamics of h_r, given by Eq. 2.47c and the SPM flow dynamics of q_{ssp} as given in Eq. 2.47f. The subset of states are reproduced below for convenience.

$$\dot{h}_r = \frac{q_{ssp} - (q_{bit} + q_{boostIn} + q_{tf})}{A_a(h_r)} \tag{2.48a}$$

$$\dot{q}_{ssp} = \frac{1}{M_{MRL}(h_r)}(P_{SPM_{IN}}(h_r) + \Delta P_{SPM}(\omega_{ssp}, q_{ssp}) - p_0 - F_{MRL}(q_{MRL}) - G_{MRL}) \tag{2.48b}$$

The various expressions included in the MRL flow rate dynamics are for convenience summarized below, gathered from the derivations in previous sections.

The pressure at the MRL inlet, $P_{SPM_{IN}}(h_r)$ can be calculated directly from the riser level as stated in Eq. 2.44

$$P_{SPM_{IN}}(h_r) = p_0 + \rho g \cdot (h_{SPM_{IN}} - h_r) \tag{2.49}$$

and the generated pump pressure is straightforwardly available from the pump head model in Eq. 2.28

$$\Delta P_{SPM}(\omega_{ssp}, q_{ssp}) = \rho g \Delta H_{SPM} = \rho g \cdot (c_0 \omega_{ssp}^2 - c_1 \omega_{ssp} q_{ssp} - c_2 q_{ssp}^2) \tag{2.50}$$

The frictional pressure losses in the MRL are assumed to be the form of the second order Taylor series polynomial as given by Eq. 2.26

$$F_{MRL} = C \cdot q_{ssp} + D \cdot q_{ssp}^2 \tag{2.51}$$

and the hydrostatic pressure contribution generated by the column of mud in the MRL was given in Eq. 2.45

$$G_{MRL} = \rho g h_{SPM_{OUT}} \tag{2.52}$$

Furthermore, the integrated density per cross-section $M_{MRL}(h_r)$ can be calculated as given by Eq. 2.46

$$M_{MRL}(h_r) = \frac{\rho \cdot (h_{SPM_{IN}} - h_r)}{A_a} + \frac{\rho \cdot h_{SPM_{OUT}}}{A_{MRL}} \tag{2.53}$$

where all parameters are known from Table 2.2.

Because of no difference in elevation between the subsea pump inlet and outlet, ($h_{SPM_{IN}} = h_{SPM_{OUT}}$), the constant hydrostatic term $\rho g \cdot h_{SPM_{IN}}$ from Eq. 2.49 cancels out G_{MRL} in Eq. 2.48b. Two terms of the atmospheric pressure at each side of the SPM also cancel out. Also, applying the input flow variables q_p and q_{bp} as approximations for the unavailable flow rate states q_{bit} and $q_{boostIn}$ in the drill string and the booster line, the final expression for the state-space system to be used as basis for system identification in Chapter 3 can be stated as

$$\dot{h}_r = \frac{q_{ssp} - (q_p + q_{bp} + q_{tf})}{A_a} \tag{2.54a}$$

$$\dot{q}_{ssp} = \frac{1}{M_{MRL}(h_r)} \left[\rho g \cdot (c_0 \omega_{ssp}^2 - c_1 \omega_{ssp} q_{ssp} - c_2 q_{ssp}^2) - (C \cdot q_{ssp} + D \cdot q_{ssp}^2) - \rho g h_r\right] \tag{2.54b}$$

Chapter 3

System Identification of Parameters not Relying on Dynamics

Now that a hydraulic model of the MRL dynamics in a dual gradient drilling system has been derived, recorded field data can be applied to estimate the unknown parameters associated with the models for the subsea pump performance and for the return line frictional losses. The subsea pump module, on one hand, and the MRL flow section, on the other, can be treated as two isolated subsystems with independent characteristics. Parameter estimation can therefore be performed in a separated fashion, consistent with the *Divide & Conquer* principle.

The generated pump pressure as well as the frictional pressure losses were in the modeling of Chapter 2 both assumed to be quantities that do not rely on dynamics. Also, since the measurements are available as priorly sampled observations, the estimation problems have a discrete-time nature. Therefore the identification will not require a continuous-time, online estimation routine, but can be based on offline (non-recursive) steady-state analysis.

This chapter aims to identify all unknown parameters of the model in Eq. 2.54 that applies to the DGD facilities in the Gulf of Mexico whence field data are provided by Statoil. Along with the parameter estimation process, the chapter also addresses validation and falsification of the assumed model structures, and proper modifications are suggested in the case of unsatisfactory initial identification results.

3.1 Offline Least Squares Method

This section aims to give a brief introduction to one of the most basic yet widely used results in parameter estimation, namely the nonrecursive least squares method. The method is described in a large amount of literature sources, e.g. Ioannou and Sun [2012], where

the link to the continuous-time recursive least squares algorithm also is thoroughly discussed. The basic idea behind the method is fitting a mathematical model to a sequence of observed data by minimizing the sum of squares of the difference between the observed and computed data. The derivation of the method is summarized below.

Suppose a certain model structure $\mathcal{M}$ is parametrized using the parameter vector $\theta \in \mathcal{D}_{\mathcal{M}} \subset \mathbb{R}^d$, yielding the set of candidate models

$$\mathcal{M}^* = \{\mathcal{M}(\theta) \,|\theta \in \mathcal{D}_{\mathcal{M}}\} \tag{3.1}$$

The search for the best model then becomes a problem of estimating θ. An approach to estimate parameters based on minimization of prediction-error is presented in Ljung [1999], and results in a scheme to find the *least-squares estimate (LSE)* of the unknown parameter vector. The reasoning behind the method is summarized below.

The prediction error given by a certain model $\mathcal{M}(\theta^*)$ is given by

$$\varepsilon(t, \theta^*) = y(t) - \hat{y}(t|\theta^*) \tag{3.2}$$

When the data set $\mathbb{Z}^N$ is known, these errors can be computed for $t = 1, 2, ..., N$. A good model is one that is good at predicting, i.e. one that produces small prediction errors when applied to the observed data. The prediction-error sequence can be viewed as a vector in $\mathbb{R}^N$, whose size can be measured using any norm in $\mathbb{R}^N$. This can be formulated as

$$V_N(\theta, \mathbb{Z}^N) = \frac{1}{N} \sum_{t=1}^{N} l(\varepsilon(t, \theta)) \tag{3.3}$$

where $l(\cdot)$ is a scalar-valued positive function. The function $V_N(\theta, \mathbb{Z}^N)$ is now a function of $\theta \in \mathcal{D}_{\mathcal{M}} \subset \mathbb{R}^d$, and a natural measure of the validity of the model. The estimate $\hat{\theta}_N$ is defined by the minimization of (3.3):

$$\hat{\theta}_N = \arg \min_{\theta \in \mathcal{D}_{\mathcal{M}}} V_N(\theta, \mathbb{Z}^N) \tag{3.4}$$

For a system with a linear regression model structure, the predictor can be written as

$$\hat{y}(t) = \varphi^\top(t)\hat{\theta}_N \tag{3.5}$$

which results in the model predictor error

$$\varepsilon(t, \theta) = y(t) - \hat{y}(t) = y(t) - \varphi^\top(t)\hat{\theta}_N \tag{3.6}$$

Here, $\varphi(t)$ is the vector of known signals, known as the *regression vector*. In this situation, when the underlying model structure is linear in θ, a particularly simple case arises. Measuring the size of the prediction-sequence error using the quadratic norm, $l(\varepsilon) = \varepsilon^2/2$, yields

$$V_N(\theta, \mathbb{Z}^N) = \frac{1}{2N} \sum_{t=1}^{N} \left(y(t) - \varphi^T(t)\hat{\theta}_N\right)^2 \tag{3.7}$$

This is the *least-squares criterion* for the linear regression in Eq. 3.5. It is quadratic in θ, allowing the optimization problem to be solved analytically in closed form. The estimate is re-denoted as $\hat{\theta}_N^{LS}$ to emphasize the least-squares approach, and is found by straightforward differentiation as

$$\theta_N^{LS}(\mathbb{Z}^N) = \arg\min_{\theta \in \mathcal{D}_\mathcal{M}} V_N(\theta, \mathbb{Z}^N) = \left[\frac{1}{N}\sum_{t=1}^{N}\varphi(t)\varphi^\top(t)\right]^{-1}\frac{1}{N}\sum_{t=1}^{N}\varphi(t)y(t) \tag{3.8}$$

The solution only exists provided the inverse exist. This normally requires the input to be *persistently exciting (PE)*, meaning that a sufficient degree of variation in the observed regression vector is needed. A comprehensive discussion of the concept is given in Ljung [1999].

3.2 Masking of Confidential Measurements

The provided field data series from Statoil ASA represent sensitive information. For this reason, identified models for the frictional losses in MRL or the subsea pump head cannot be revealed in their original form. A convention is defined in order to transform variables from their original units into percentage of some unknown value corresponding to $100\,\%$, where the unknown value definitions for the various variables are hidden for the reader.

The frictional losses, originally measured in Pa, are transformed into frictional losses measured in percentage of some unknown value corresponding to $100\,\%$. This conversion can be written mathematically as

$$F[\%] = \frac{F[Pa]}{F_{100\%}[Pa]} \cdot 100 \tag{3.9}$$

Similarly, all flow rates, originally measured in $\frac{\mathrm{m}^3}{\mathrm{s}}$, are transformed into percentage of some unknown value corresponding to $100\,\%$ according to

$$q[\%] = \frac{q[\frac{\mathrm{m}^3}{\mathrm{s}}]}{q_{100\%}[\frac{\mathrm{m}^3}{\mathrm{s}}]} \cdot 100 \tag{3.10}$$

For pump head, the conversion is written out as

$$\Delta H_{SPM}[\%] = \frac{\Delta H_{SPM}[m]}{H_{100\%}[m]} \cdot 100 \tag{3.11}$$

and for the riser level, the conversion is written

$$h_r[\%] = \frac{h_r[m]}{h_{r_{100\%}}[m]} \cdot 100 \tag{3.12}$$

3.3 Frictional Pressure Losses in Mud Return Line

As described in Section 2.3, the frictional losses along any flow section can be described as a function of the flow rate. The complete mud return line can be divided into three sections where frictional losses could occur to a varying degree; the suction line, which is the inlet to the SPM from the riser, the discharge line, which extends from the SPM outlet and up to the rig floor, and lastly, the subsea pump module itself. The suction line is assumed to be very short, which justifies neglecting frictional losses in this section. The frictional losses in the pump are integrated in the model of the pump performance function as described in Section 2.4, and will not be considered here. This section will therefore deal solely with the frictional pressure losses at the outlet side of the SPM.

The available field data provide insight into flow and pressure conditions of the mud return line, and a schematic of the relevant transmitters is shown in Figure 3.1. Two redundant pressure transmitters are averaged to give a measure of the pressure at the outlet of the SPM. The transmitter for the flow is placed at the flow line at rig level. The volume flow rate through the MRL is assumed not to vary spatially within the MRL, meaning that the flow rate at all locations is believed to match the measured volume flow at the rig floor, q_{MRL}, at any given time. Therefore the flow rate that will be used in the parameter estimation is the actual measurement q_{MRL}, but the friction model is still written as a function of the flow rate through the subsea pump, which is state variable q_{ssp}.

The observed frictional pressure losses of the MRL can be calculated from the field data in a straightforward manner. The pressure difference between the SPM outlet and the MRL outlet must exclusively be a combination of hydrostatic difference and the frictional losses. To calculate the size of the frictional losses from the field data at any given time, the hydrostatic contribution from the discharge line, which is assumed to be constantly filled with mud, must therefore be subtracted from the pressure difference, yielding

$$F_{MRL} = P_{SPM_{OUT}} - \rho g h_{SPM_{OUT}} - p_0 \tag{3.13}$$

3.3.1 Least squares estimate of friction model coefficients

The second order polynomial model for the MRL frictional losses as a function of flow rate was suggested in Eq 2.51. Substituting the flow state variable q_{ssp} with the flow measurement q_{MRL} in purpose of parameter estimation yields the model

$$F_{MRL} = C \cdot q_{MRL} + D \cdot q_{MRL}^2 \tag{3.14}$$

The friction model in Eq. 3.14 is linear in its unknown coefficients, and can be restated using a linear regression structure as described in Section 3.1. This yields

$$y(t) = \varphi^T(t)\theta^* \tag{3.15}$$

where

$$\varphi(t) = [q_{MRL}(t),\ q_{MRL}^2(t)]^\top \tag{3.16}$$

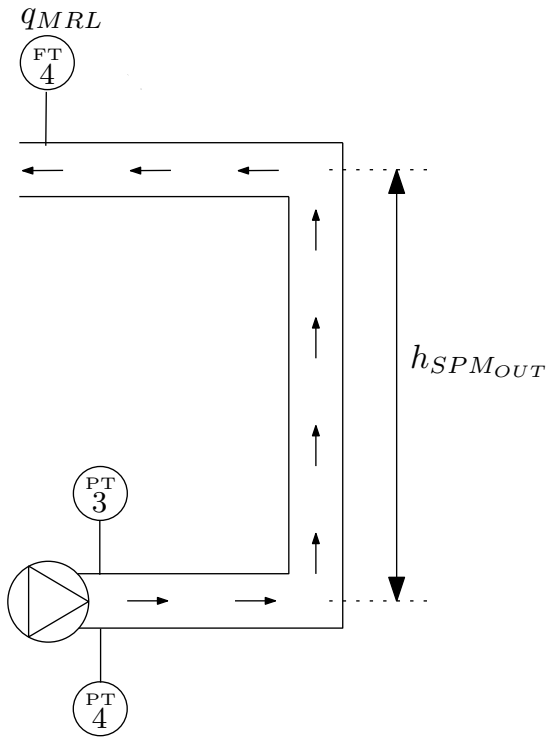

Figure 3.1: Schematic of mud return line transmitters and associated measurements.

is the regression vector of known signals at time t,

$$\theta^* = [C^*,\ D^*]^\top \tag{3.17}$$

is the unknown parameter vector and

$$y(t) = F_{MRL}(t) \tag{3.18}$$

is the measurement variable at time t. The linear regression employs the predictor

$$\hat{y}(t) = \varphi^\top(t)\hat{\theta} \tag{3.19}$$

that is linear in θ, enabling the use of the least squares method that is summarized by the expression in Eq 3.8 in Section 3.1 in order to identify θ_N^{LS}.

Prior to finding the LSE of the coefficients, all data in four consecutive field data series {gom1, gom2, gom3, gom4} can be plotted to give an unpolished overall picture of the relationship between the observed MRL flow rate and the observed frictional losses as calculated from Eq. 3.13. The data span a time interval of almost 85 hours, sampled at a frequency of 1 Hz, yielding the total number of 305820 data points. A few outliers outside the frame are not shown in order to achieve appropriate zoom and increased readability. The data points are plotted below in Fig. 3.2.

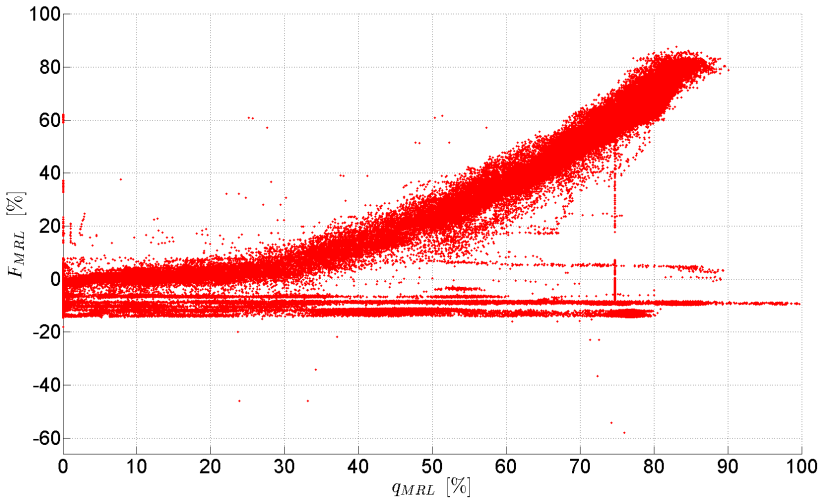

Figure 3.2: Observed MRL flow rate plotted against the frictional pressure losses in the MRL (all data).

Several observations can be made from this plot of raw data. A considerable amount of sample points for a wide range of flow rates indicate that the total frictional losses are negative, which of course is physically impossible. These data points originate from the fact that the pressure at the SPM outlet is measured to be less than the pressure the full hydrostatic column of mud would exert, which clearly means that the assumption of a filled return line in the calculation of the frictional pressure losses does not hold. A likely explanation for these erroneous friction observations is that the top of the discharge line is somewhat emptied of mud due to the occurring difference in flow rate in and flow rate out of the discharge line just as the pump shuts off, making the calculation of friction from Eq. 3.13 invalid for some time instants. By disregarding these data points in the figure, a quadratic relationship between flow rate and frictional losses is however indicated by the rest of the data. These observations suggest that rejecting potentially erroneous or inapplicable data is essential in order to obtain a data set that will yield a realistic model of the frictional losses from least squares fitting. The applied data should be gathered from time intervals during regular operations in the mud return line, requiring that:

- The pump is on ($\omega_{ssp} > 0$).
- The pump generates a positive pressure increase ($\Delta P_{SPM} > 0$).
- The pump flow is positive ($q_{MRL} > 0$).

Data that don't meet these requirements are ignored in the calculations of the frictional model to follow. In addition, it is observed by manual inspection that several intervals containing consecutive perfectly equal flow rate measurements or pump speed measure-

ments exist, as if the measurements were stuck or have failed to update. Data that still don't belong to the collection of points that constitute the quadratic-like curve, tend to belong to these sets of measurement, so these measurements are removed as well. The remaining 52579 data points are plotted in blue together with the underlying plot of the full data series marked by red in Fig. 3.3 below.

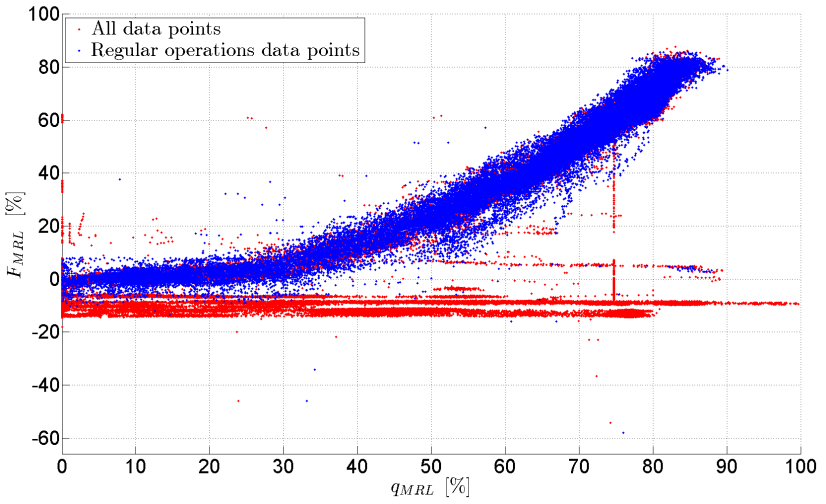

Figure 3.3: Observed MRL flow rate plotted against the frictional pressure losses in the MRL.

It is evident from quick visual inspection that this screening of inapplicable data yields a seemingly quadratic relationship between the flow rate and the frictional pressure losses in the MRL. Also, a huge majority of the sample points indicating negative friction have been discarded. There are still remaining blue sample points that indicate negative frictional losses, especially for low flow rates. Possible explanations are calibration errors of the pressure transmitters and unmodeled high-frequency fluctuations in pressure due to turbulence connected to pump shut-off and shut-on.

MATLAB provides the built-in least-squares solver `lscov`, which finds the least-squares solution x to the linear system of equations $Ax = b$. For this problem of estimating the frictional coefficients, A will be a matrix of dimension $(n \times d)$, where n is the length of the series of applied measurements and each row i is the regression row vector $\varphi(i)$ of size $d = 2$, as given by Eq. 3.16. Each index i in the vector b is $y(i)$, as given by Eq. 3.18. The unknown coefficients are returned in the vector $x = \theta_N^{LS}$. The function also returns the estimated standard errors of x, and the mean squared error. Complementary documentation of the `lscov` function is readily available in MathWorks [2015c].

A MATLAB function was written to select the applicable field data from time intervals of regular operations and calculate the least squares estimates of the friction model coefficients. The plot of the data points applied in the least squares estimation along with the

resulting friction model curve is shown below in Figure 3.4.

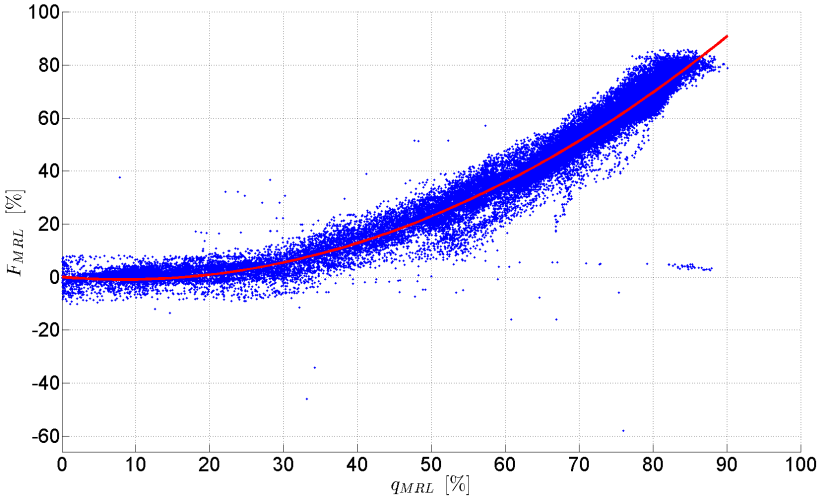

Figure 3.4: Frictional pressure losses in the MRL as a function of flow rate, given by the model in Eq. 3.14.

The mean squared error for the model is found to be

$$MSE = 21.89 \tag{3.20}$$

3.3.2 Least squares estimate of friction model coefficients assuming time delay in flow rate measurement

In the introduction of Section 3.3, the assumption of flow rate that does not vary spatially within the MRL, was restated. The applied argument up until now has been that density effects in flow are likely only to have minor effects for relatively low fluid velocities, making the fluid accelerate homogeneously as a stiff mass. However, the distance between the transmitter and a random reference point along the return line could in principle give rise to some time delay in the measurement of the flow rate of that point due to pressure transients that propagate as pressure waves in the fluid along its path. Also, unmodeled dynamics are connected the Non-Newtonian properties of the oil-based mud, which cause some uncertainty in the behavior of the flow through the MRL. Due to the spread in the friction measurements for each flow rate, these assumptions should be set to the test.

A new hypothesis is the following: The frictional losses should not be fitted to the return flow measurement q_{MRL} of the same time instant, but to some unmeasured flow rate $\hat{q}_{MRL}$ at an unknown point in the middle of the MRL that can be approximated as the measurement q_{MRL} at an later time instant $(t + \theta_{fric})$, yielding

$$q_{MRL}(t) = \hat{q}_{MRL}(t - \theta_{fric}), \quad \theta_{fric} > 0 \tag{3.21}$$

or equivalently

$$\hat{q}_{MRL}(t) = q_{MRL}(t + \theta_{fric}), \quad \theta_{fric} > 0 \tag{3.22}$$

The following modification to the model in Eq. 3.14 is therefore suggested

$$F_{MRL}(t) = C \cdot q_{MRL}(t + \theta_{fric}) + D \cdot q^2_{MRL}(t + \theta_{fric}) \tag{3.23}$$

The validity of the model in Eq. 3.23 can be tested by calculation of the MSE value of the least squares estimation for various values of the time delay θ. For time delay values in the set $\{\theta_{fric} \in \mathbb{Z} : \theta_{fric} \in [0, 30]\}$, the flow rate measurement vector is shifted forward with θ_{fric} seconds in the calculation of F_{MRL}, and an individual least squares fit is performed for each value of θ_{fric}. The MSE values for the given range are plotted below in Figure 3.5.

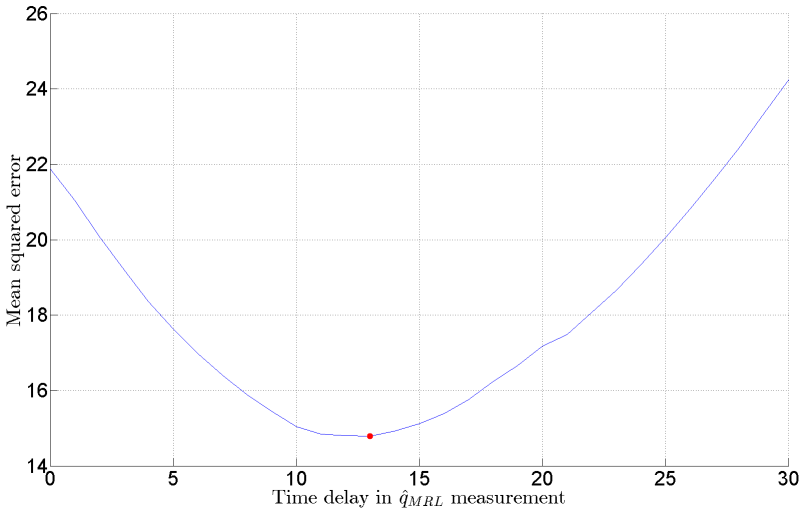

Figure 3.5: Mean squares error from the LSE fit of the model in Eq. 3.23 for various values of the time delay θ_{fric}.

The lowest MSE values is obtained for $\theta_{fric} = 13\,\mathrm{s}$ and is returned as

$$MSE = 14.79 \tag{3.24}$$

The unmeasured flow rate $\hat{q}_{MRL}$ is therefore redefined more specifically as

$$\hat{q}_{MRL}(t) = q_{MRL}(t + 13) \tag{3.25}$$

The plot of time shifted flow rate data $\hat{q}_{MRL}$ against the calculated frictional losses applied in the least squares estimation is shown below in Fig 3.6 along with the resulting friction model curve.

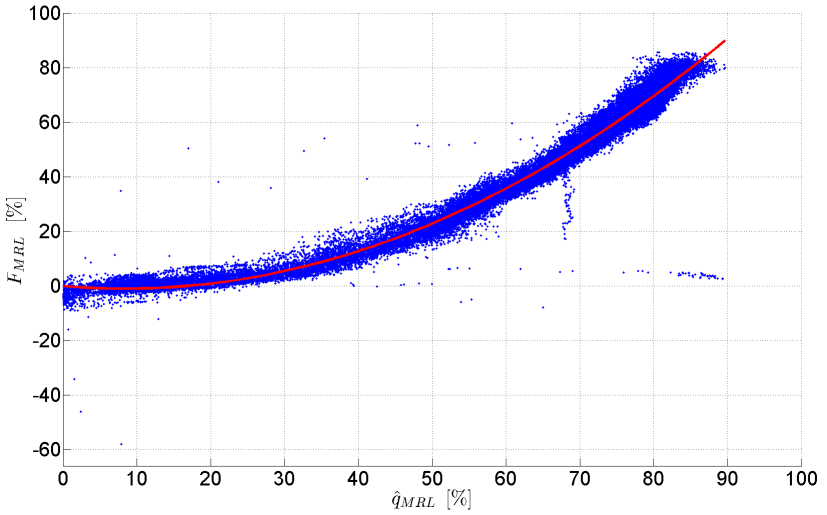

Figure 3.6: LSE fit of the model in Eq. 3.23 for time delay $\theta_{fric} = 13\,\mathrm{s}$.

The LSE of the coefficients of the model in Eq. 3.23 are close to identical to those obtained in for the model in Eq. 3.14. However, by visual inspection it is obvious that this modified model seems to represent an appreciable and reasonable improvement, as the sample points are much tighter fitted around the found model curve, giving rise to a lower MSE value.

Still, due to the linear coefficient C being negative-valued, the fitted model yields negative frictional losses for a certain interval of low flow rate values. The set of data points in Figure 3.6 suggests however by visual inspection that the frictional pressure losses should be a function strictly increasing with flow. The negative value of the linear coefficient seems to result from the restrictions in curvature of a second order polynomial. The time delay modification is kept in the model, but additional flexibility is achieved by replacing the linear term with a constant term to open for offset in the model due to calibration errors in the pressure measurements. In addition, a third order term is introduced for increased curvature flexibility. This yields the modified model

$$F_{MRL} = B + D \cdot \hat{q}^2_{MRL} + E \cdot \hat{q}^3_{MRL} \tag{3.26}$$

Using a linear regression structure, this yields the new regression vector at time t

$$\varphi(t) = [1,\ \hat{q}^2_{MRL}(t),\ \hat{q}^3_{MRL}(t)]^\top \tag{3.27}$$

and the unknown parameter vector

$$\theta^* = [B^*,\ C^*,\ D^*]^\top \tag{3.28}$$

Calculation of the least squares estimate of the coefficients yield the MSE value of

$$MSE = 14.61 \tag{3.29}$$

which is a slight improvement compared to the value from the quadratic model found in Eq. 3.24.

The friction model curve is shown below in Figure 3.7 together with the applied data points of the least squares estimation. The function is strictly increasing due to the positive coefficients of the quadratic and cubic terms, and will serve as the final outcome of this identification process of the frictional losses model in the MRL.

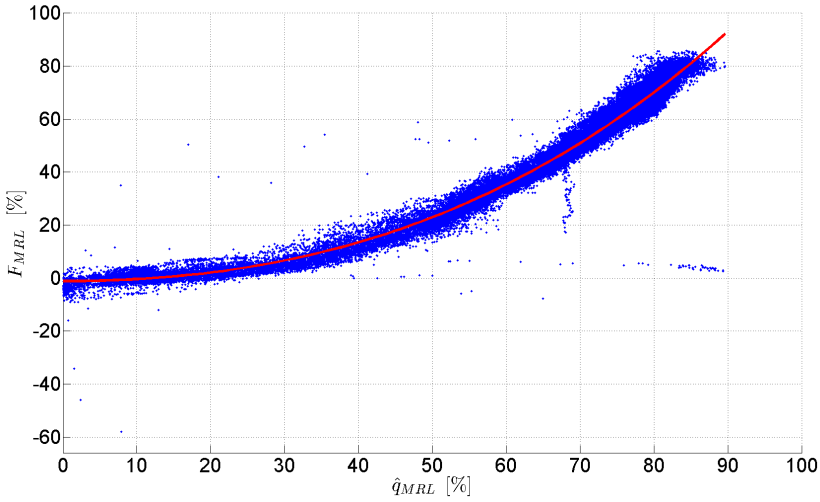

Figure 3.7: LSE fit of the frictional losses model in Eq. 3.26.

3.4 Subsea Pump Performance Characteristics

As described in Section 2.4, the subsea pump can be characterized by its pump performance curve, which is the mathematical model of the generated pump head as a function of the pump rotation speed and mud flow rate through the pump.

The available field data provide detailed insight into the conditions in the mud return line. A schematic of the transmitters along the MRL section, relevant to the subsea pump performance, is shown in Figure 3.8. Measurements from redundant pressure transmitters are averaged to give an accurate measure of the pressure both at the inlet ($P_{SPM_{IN}}$) and the outlet ($P_{SPM_{OUT}}$) of the SPM. Since the inlet and outlet are placed at the same elevation depth, the generated pump pressure ΔP_{SPM} is easily calculated as the pressure increase from the inlet side to the outlet side.

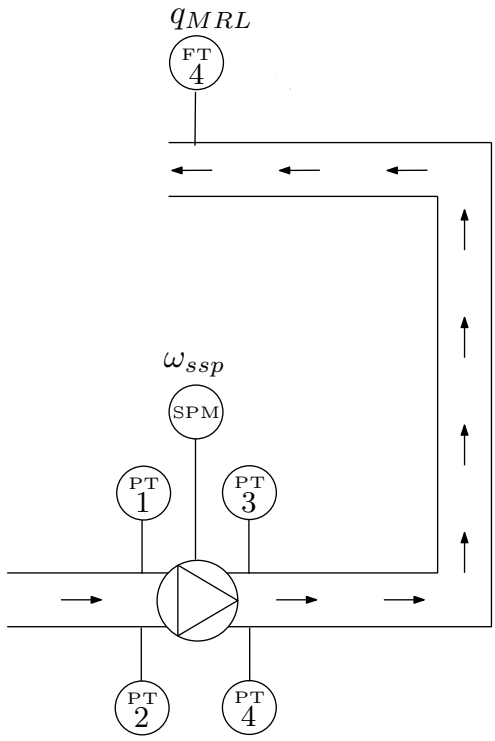

Figure 3.8: Schematic of Mud Return Line transmitters and associated measurements.

As demonstrated in Section 3.3, it eventually seemed beneficial to model the frictional pressure losses in the MRL as a function not of the flow measurement q_{MRL}, but of some unmeasured flow rate $\hat{q}_{MRL}$ at some unspecified point in the MRL that could be approximated as the measured q_{MRL} at a later time instant $(t + \theta_{fric})$. This modification was based on rejection of the initial assumption that the flow rate does not vary spatially within the MRL. It is reasonable to assume that a similar modification applies to the modeling of the pump performance characteristics. The initial assumption in connection to subsea pump performance is that the flow rate through the subsea pump, q_{ssp} can be estimated as the unmeasured flow rate $\hat{q}_{MRL}$, mathematically stated as:

$$q_{ssp}(t) = \hat{q}_{MRL}(t) = q_{MRL}(t + 13) \tag{3.30}$$

Together with logged measurements of the subsea pump speed, ω_{ssp}, the pressure and flow measurements provide all the components of information needed to find a characterization of the subsea pump curve. The assumed function for the pump head was given in Eq. 2.28 in Chapter 2 and is reproduced below for convenience.

$$\Delta H_{SPM}(\omega_{ssp}, q_{ssp}) = c_0\omega_{ssp}^2 - c_1\omega_{ssp}q_{ssp} - c_2q_{ssp}^2 \tag{3.31}$$

The model in Eq. 3.31 takes a form that allows for restating using a linear regression model structure, where the unknown parameters and the known measurements are collected in

respective vectors. This yields

$$y(t) = \varphi^T(t)\theta^* \tag{3.32}$$

where

$$\varphi(t) = [\omega_{ssp}^2(t), -\omega_{ssp}(t)q_{ssp}(t), -q_{ssp}^2(t)]^\top \tag{3.33}$$

is the regression vector of known signals at time t,

$$\theta^* = [c_0^*, c_1^*, c_2^*]^\top \tag{3.34}$$

is the unknown parameter vector and

$$y(t) = \Delta H_{SPM}(t) \tag{3.35}$$

is the measurement variable at time t. The linear regression employs the predictor

$$\hat{y}(t) = \varphi^\top(t)\hat{\theta} \tag{3.36}$$

that is linear in θ, enabling the use of the least squares method that was described in Section 3.1 in order to find the vector of the unknown parameters.

3.4.1 Least squares estimate of pump characteristics coefficients

Before GoM field data is applied to solve for the least-squares estimates of the pump curve coefficients, the same rejection of inapplicable data is performed as in connection to the estimation of the friction model.

Similar to the friction model estimation, the build-in least-squares solver `lscov` in MATLAB is used to find the least-squares solution x to the linear system of equations $Ax = b$. For this problem of estimating the pump model coefficients, A will be a matrix of dimension $(n \times d)$ where n is the length of the series of applied measurements and each row i is the regression row vector $\varphi(i)$ of size $d = 3$, as given by Eq. 3.33. Each index i in the vector b is $y(i)$, as given by Eq. 3.35. The unknown coefficients are returned in the vector $x = \theta_N^{LS}$.

A MATLAB function was written to select the applicable field data and calculate the least squares estimates of the pump characteristics coefficients. The mean squared error for the model is found to be

$$MSE = 1.3907 \tag{3.37}$$

Figure 3.9 shows the pump curves for an evenly spaced set of values for the pump rotation speed ω_{ssp} in the interval $30\% - 70\%$ of full rotation speed, where the most field data are found. The original field data points in vicinity of each speed value $(\omega_{ssp}(i) \pm 0.1)\%$ are plotted with matching color.

Immediately a visual inspection of Fig. 3.9 reveals that this least-squares fit does not seem to yield an appropriate pump head model, as the deviation between the pump curves and the corresponding field data points are quite large for many rotation speeds. This can be

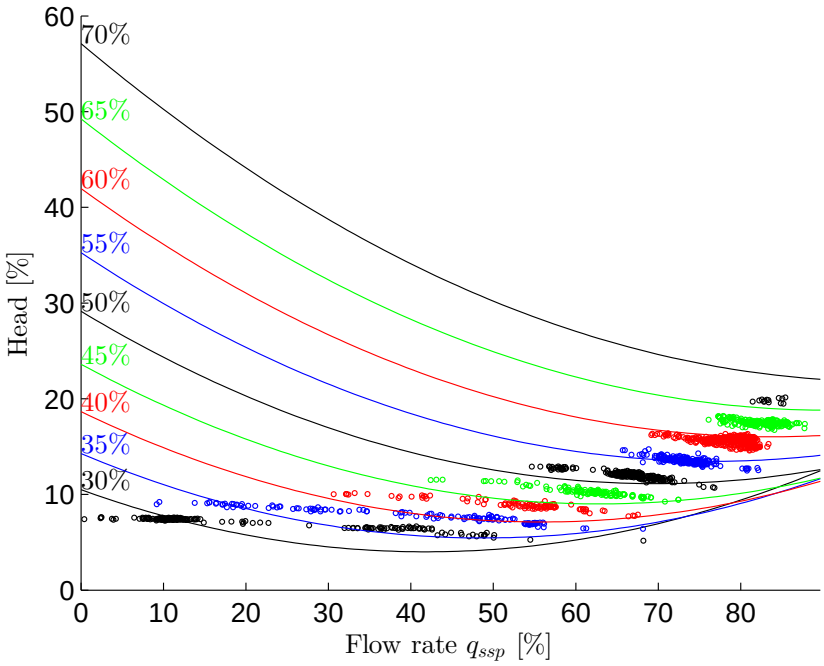

Figure 3.9: Pump performance curves obtained by LSE fitting of the model in Eq. 3.31.

explained by the coefficient c_2 being negative, which gives rise to pump curves that are convex, due to the positive sign of the double derivative of the head function w.r.t. flow rate:

$$\frac{\partial^2 \Delta H_{SPM}}{\partial q_{ssp}^2} = -2c_2 > 0 \tag{3.38}$$

This essentially means that the pump head will eventually start to increase with higher flow rates. This is neither physically realistic nor consistent with the theory from Section 2.4, which states that there is a maximum flow rate corresponding to each given pump speed, at a point where the head is zero, referred to as the pump's free delivery. Hence, a correct pump curve cannot be convex. All together, this argues in favor of rejection of this model and the found pump curves in Figure 3.9.

Important for the accuracy and reliability of any least squares fit is the richness of the measurement data, as discussed in Section 3.1. For a given pump speed, there should ideally exist flow rate data to span the whole interval between very low flow rate up until significant flow. For the data used in this least-squares fitting, it is obvious that most points for each given pump speed is gathered within a small flow interval. This creates a high level of uncertainty in the form of the curve. A modified attempt to obtain a better fit of the model is to base the least squares estimate solely on data of pump speeds which includes corresponding flow rate measurements that span a larger interval. From Fig. 3.9 it can be

noticed that this seem to yield for the low rotational speeds. By further inspection, a figure of ω_{ssp} plotted against q_{ssp} shows that richer flow data exist for $\omega_{ssp} \in [20, 40]$. However, only using these data in the fit does not contribute to a more valid result, as the resulting pump curves are still convex. This attempt will not be discussed in further detail.

To obtain a least-squares fit that yields a more realistic model for the pump curves, adjustment to the model structure in Eq. 3.31 should be considered. The distance between adjacent pump curves in Fig. 3.9 from the least squares fit seems larger than the field data suggest, an observation which motivates us to try to reduce the order of the terms in the model. By introduction of new degrees of freedom in the values of the exponents, it should be possible to find least-squares fitted pump curves that are concave and decreasing until the flow rate at the pump's free delivery point. An approach to find a modified polynomial model is outlined in the subsection to follow.

3.4.2 Search for modified pump characteristics model

The pump curve model is modified to

$$\Delta H_{SPM}(\omega_{ssp}, q_{ssp}) = c_0 \omega_{ssp}^{n0} - c_1 \omega_{ssp} q_{ssp} - c_2 q_{ssp}^{n2} \tag{3.39}$$

which gives two new DOFs in the unknown exponents, n_0 and n_2.

For a given set of exponent values (n_0, n_2), the LSE coefficients can be found easily by performing a least squares fitting the same way as in Subsection 3.4.1. In order to find the exponent values of the most appropriate model in a reasonable amount of time, a search should be structured mathematically. One way of doing this is to employ a numerical optimization algorithm to perform a search in direction of the set of exponent values that yield a least squares fitted model which at best replicates the observed data. This can be obtained by defining the mean squared error as the objective criterion in the optimization routine to be minimized. Since no expression for the derivative of the the MSE is obvious, a derivative-free method is appropriate. The MATLAB function `fminsearch` applies the Nelder-Mead method to find a local minimum of a given objective function.

The Nelder-Mead method is described in detail in Nocedal and Wright [2006], and is roughly summarized here for convenience. The method is popular due to its intuitive nature, and works by keeping track of $n + 1$ points of interest in $\mathbb{R}^N$, whose convex hull forms a simplex. In each iteration, the algorithm seeks to remove the vertex with the worst objective value and replace it with another point with a better value. The new point is obtained by reflection, expansion or contraction of the simplex. Documentation of the `fminsearch` function is readily available in MathWorks [2015a].

Nelder-Mead is an unconstrained optimization routine, which in principle will perform the search for (n_0, n_2) in the full $\mathbb{R}^2$. However, the main reason for considering the change in the pump model of Eq. 3.31 in the first place, was to obtain a pump characteristics expression which ensured that the head was decreasing in flow rate and concave in shape. Thus some measures must be taken to constrain the optimization routine from choosing exponents that yield unrealistic pump characteristics.

The properties of a monotonically decreasing and concave shape can be translated into constraints on the unknown parameters in the expression in Eq. 3.39. First, the negative derivative requirement yields that

$$\frac{\partial \Delta H_{SPM}(\omega_{ssp}, q_{ssp})}{\partial q_{ssp}} = \frac{\partial \left(c_0 \omega_{ssp}^{n0} - c_1 \omega_{ssp} q_{ssp} - c_2 q_{ssp}^{n2}\right)}{\partial q_{ssp}} \tag{3.40}$$

$$= -c_1 \omega_{ssp} - n_2 c_2 q_{ssp}^{n_2 - 1} < 0 \tag{3.41}$$

The expression must hold in the limit as $q_{ssp} \to 0$, yielding that $c_1 > 0$. In the limit that $\omega_{ssp} \to 0$, the expression must also hold, meaning that $n_2 c_2 > 0$.

Secondly, the concave property is ensured if the second derivative is less than zero, which requires that

$$\frac{\partial^2 \Delta H_{SPM}(\omega_{ssp}, q_{ssp})}{\partial q_{ssp}^2} = \frac{\partial \left(-c_1 \omega_{ssp} - n_2 c_2 q_{ssp}^{n_2 - 1}\right)}{\partial q_{ssp}} \tag{3.42}$$

$$= -(n_2 - 1) n_2 c_2 q_{ssp}^{n_2 - 2} < 0 \tag{3.43}$$

Assuming that the requirement $n_2 c_2 > 0$ has already been met means that $n_2 > 1$ is also required for the pump curve to be concave. Since $n_2 > 1 > 0$, this also means that $c_2 > 0$ to satisfy the inequality $n_2 c_2 > 0$. To summarize, this reasoning yields the following constraints

$$c_1, c_2 > 0, \; n_2 > 1 \tag{3.44}$$

The search for an optimized model structure can be summarized as the following procedure:

Algorithm to search for optimal exponents of the pump curve model in Eq. 3.39

1. Start search with a guess of (n_0, n_2).
2. Find least squares estimates of pump head model coefficients with current exponent values and calculate MSE. Set objective function value to MSE.
3. Ensure that pump curve shape criteria in Eq. 3.44 are complied. Change objective function value to infinity if the criteria are not held.
4. Let optimization routine choose (n_0, n_2) of next iteration based on the information of the new objective value.
5. Repeat points 2-4 until optimization converges to a point (n_0^*, n_2^*).

For a proper initial guess of exponent values, the resulting search path of the algorithm is shown in Fig. 3.10.

With the optimized exponents, the LSE fitting yields the $MSE = 0.071$. The resulting pump performance curves are shown below in Figure 3.11.

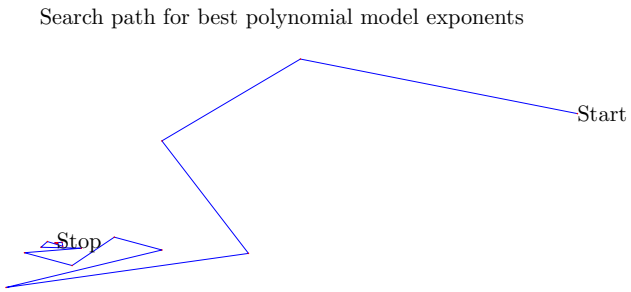

Figure 3.10: Search path of the outlined search algorithm

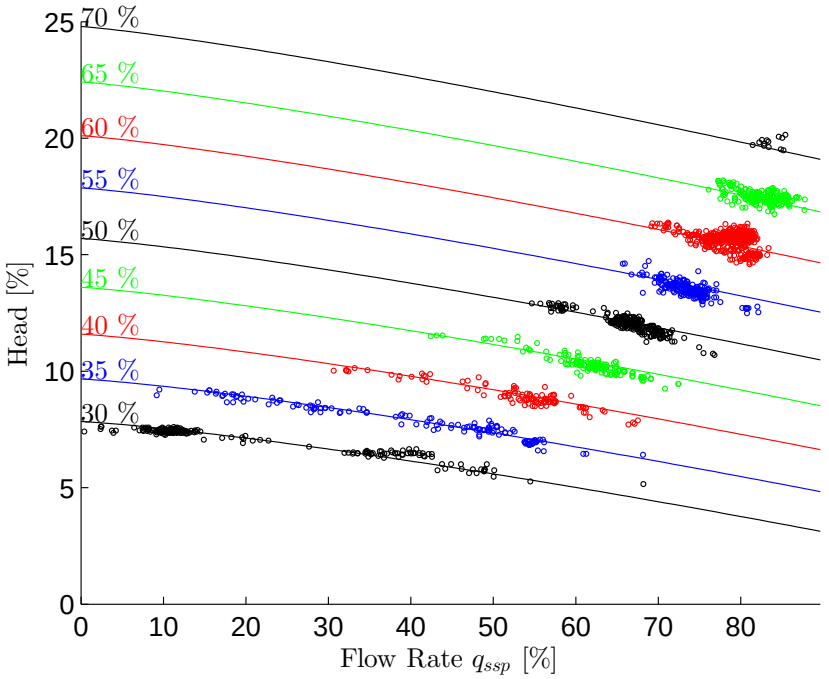

Figure 3.11: Pump performance curves for the LSE fitted model in Eq. 3.31 with optimized exponents.

By comparison of Fig. 3.11 and Fig. 3.9, the improvement of the modified model is conspicuous. The mean squared error is significantly lower, yielding a seemingly very accurate model of the pump performance. This model will serve as the final outcome of this identification process of the pump performance characteristics.

3.5 Total System Description of Mud Return Line Dynamics

The various findings from the system identification process of this chapter have altered the structure of the dynamical models that was used as a basis for the system description somewhat. The original state-space system from Eq. 2.54 that rounded off the previous chapter can now be written in the modified form that will be used in the simulations of the system dynamics in Chapter 4. The system can be written as

$$\dot{h}_r = \frac{q_{ssp} - \overbrace{(q_p + q_{bp} + q_{tf})}^{q_{In}}}{A_a} \tag{3.45}$$

$$\dot{q}_{ssp} = \frac{1}{M_{MRL}(h_r)} \left[\rho g \cdot (c_0 \omega_{ssp}^{n0} - c_1 \omega_{ssp} q_{ssp} - c_2 q_{ssp}^{n2}) - (B + D \cdot q_{ssp}^2 + E \cdot q_{ssp}^3) - \rho g h_r\right] \tag{3.46}$$

Chapter 4

Simulation of Dynamics in Mud Return Line

Chapter 3 dealt with identification of the subsea pump performance characteristics and the model for the MRL frictional pressure losses. As noted, the prior assumption of flow rate not varying spatially within the return line was repudiated, resulting in a modeled time delay between the flow rate measurement, q_{MRL} and the flow through the subsea pump, q_{ssp}. Also, both the assumed model structures were somewhat altered, as they initially lead to identified models that replicated the measured outcomes poorly and gave rise to other unphysical system properties.

The dynamics of the system in Eq. 3.45 - 3.46 can now be simulated with input variables available from the recorded field data to produce times series of the state in the model. The consistency between the simulated state variables and their measured counterparts will function as a natural measure of the validity of the identified model. Potential discrepancies between simulation results and field data measurements could encourage modification or expansion of the model until the dominating dynamics seen from the field data are captured in the model to an appropriate degree of accuracy.

Before the complete dynamics are simulated as a whole, the riser level dynamics and the subsea pump flow dynamics will be simulated separately in order to better inspect the validity of each of the obtained model equations.

4.1 Riser Level Dynamics Simulation

The dynamics of the MRL in Eq. 3.45 - 3.46 are stated in a state space representation which is convenient in order to utilize the numerical solvers included in MATLAB, where the most widely used in the default solver `ode45()`. Its inner workings are outside the

scope of this thesis, but the documentation is readily available in MathWorks [2015d].

In order to simulate the riser level separately, the flow rate q_{ssp} must be provided as an input from the measured field data. The flow rates entering the riser are combined into the input variable $q_{In} = q_p + q_{bp} + q_{tf}$. The continuous riser levels dynamics of Eq. 3.45 are implemented as the MATLAB function `hr_dynamics(t,tObs,uData)`. The function is reproduced below and should be self-explanatory to most readers.

```
function Dhr = hr_dynamics(t, tgomData, uData)

global riserID drillpipeOD

% Input variables found from interpolation of data measurements at query point t
qssp = interp1(tgomData,uData(:,1),t,'linear');
qIn = interp1(tgomData,uData(:,2),t,'linear');

% Annulus cross-sectional area
Aa = pi*((riserID/2)^2 - (drillpipeOD/2)^2); % [m^2]

% hr derivative
Dhr = 1/Aa*(qssp-qIn);

end
```

The following code excerpt shows an implementation for numerical simulation of the given `hr_dynamics.m`

```
[t,hrSim] = ode45(@(t,hrSim) hr_dynamics(t,tObs,uData), tspan, hrSim0);
```

The code instructs MATLAB to simulate `hr_dynamics` over the time horizon `tspan` with the initial condition `hrSim`. The output of the function is time vector `t` and the state vector `hrSim`. The numerical simulation is performed within the written MATLAB function `sim_riser_level.m` for `tspan = [14000 20000]`, with initial condition being the measurement of the riser level at time $t = 14000s$, easily approximated from SPM inlet pressure, $P_{SPM_{IN}}$, as given below

$$h_r = h_{SPM_{IN}} - \frac{P_{SPM_{IN}} - p_0}{\rho g} \tag{4.1}$$

The simulated riser level and observed measurement are plotted in Figure 4.1 together with input flow rate variables. It can easily be observed that the simulated riser level is not consistent with the measured, but the same trends can be seen. This indicates that the structure of the differential equation for the riser level is correct, but there might be some calibration offset in the flow rate measurements.

To obtain a very consistent result in simulation of the riser level alone, should also not be expected. As the derivative is not a function of h_r itself, there is no natural feedback to restrain the state from drifting apart from the measurement in the case of inputs from badly

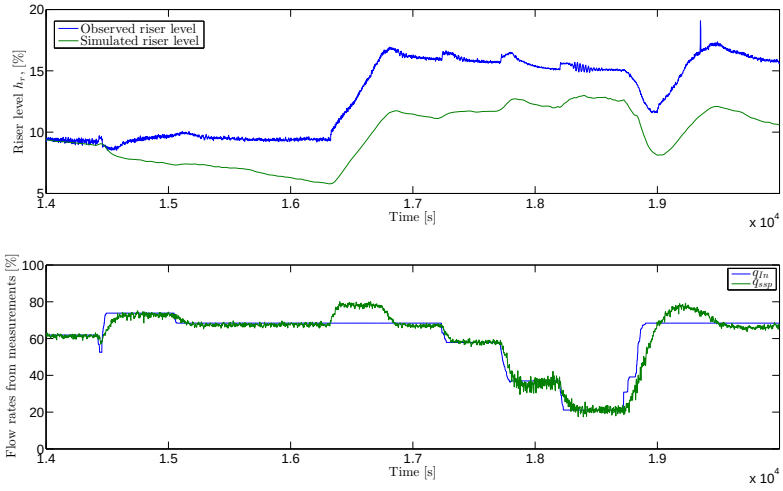

Figure 4.1: Simulation of the riser level.

calibrated flow rate measurements. It must therefore be expected that without corrective feedback from an observer, open loop simulations of the obtained model will yield state time series that are somewhat inconsistent with recorded measurements. Corrective actions will not be taken before the complete MRL dynamics are simulated.

4.2 Subsea Pump Flow Dynamics Simulation

Simulation of the SPM flow rate, q_{ssp} is performed in a very similar way the simulation of the riser level. The riser level h_r, is now provided from the measurement data, calculated as given by Eq. 4.1, along with the subsea pump speed ω_{ssp} as inputs to the system. The continuous dynamics of Eq. 3.46 are implemented in the MATLAB function `qssp_dynamics.m`. The function is reproduced below:

```
function Dqssp = qssp_dynamics(t, qssp, tgomData, uData, cCoeffs, cExps, pFric)

global g rho riserID drillpipeOD mrlID hSPMin hSPMout q100 H100 F100

% Mask parameters in [%]
qssp = qssp/q100*100;

% Input variables found from interpolation of data measurements at query point t
hr = interp1(tgomData,uData(:,1),t,'linear');
wssp = interp1(tgomData,uData(:,2),t,'linear');

% Pump pressure produced
```

```
13 c0 = cCoeffs(1);
14 c1 = cCoeffs(2);
15 c2 = cCoeffs(3);
16 n0 = cExps(1);
17 n2 = cExps(2);
18 DeltaPspm = rho*g*(H100/100)*(c0*wssp^n0 - c1*wssp*qssp - c2*qssp^n2);
19
20 % Required system head
21 B = pFric(1);
22 D = pFric(2);
23 E = pFric(3);
24 Fmrl = (F100/100)*(B + D*qssp^2 + E*qssp^3);
25 Gtot = rho*g*hr;
26
27 % Integrated density per area
28 Aa = pi*((riserID/2)^2 - (drillpipeOD/2)^2); % [m^2]
29 Amrl = pi*(mrlID/2)^2; % [m^2]
30 Mmrl = rho/Aa*(hSPMin - hr) + rho/Amrl*hSPMout; % [kg/m^4]
31
32 % qssp derivative
33 Dqssp = 1/Mmrl*(DeltaPspm - Fmrl - Gtot);
34
35 end
```

The following code excerpt shows an implementation for numerical simulation of the given `qssp_dynamics`:

```
1 [t,qsspSim] = ode45(@(t,qsspSim) qssp_dynamics(t,qsspSim,tObs,uData, ...
2     cCoeffs,cExps,pFric), tspan, qsspSim0);
```

The code instructs MATLAB to simulate `qssp_dynamics` in a similar fashion as with the riser level in Section 4.1. Additional input variables are the identified coefficients of the friction model, `pFric`, along with the coefficients, `xCoeffs`, and the exponents, `xExps`, of the pump model. The numerical simulation is performed within the the written MATLAB function `sim_flow_MRL_dynamic_eq.m` for `tspan = [14000 20000]` with initial condition being the measurement of the flow rate at time $t = 14000\,\mathrm{s}$.

The simulated and observed subsea pump flow rate are plotted in Figure 4.2. To a much larger degree than in the case for the riser level, the simulated flow rate correspond to the observed measurement. In contrast to the riser level dynamics, there exist natural feedback in the calculation of the flow rate derivative. The high level of correspondence is a good indication that the inner structure of the differential equation for the subsea pump flow rate yields a very representative description of the real flow dynamics in the GoM dual gradient drilling system.

In Kaasa et al. [2011], it is argued that the accuracy of the integrated density over area parameter M is not crucial, since it is related to the fast dynamics of the flow rate, which in most cases can be neglected. The parameter M_{MRL} was found to be in magnitude 10^7, which should correspond to very quick dynamics. To check this, the system can be simulated for steady state conditions by assuming $\dot{q}_{ssp} = 0$, which converts the dynamic

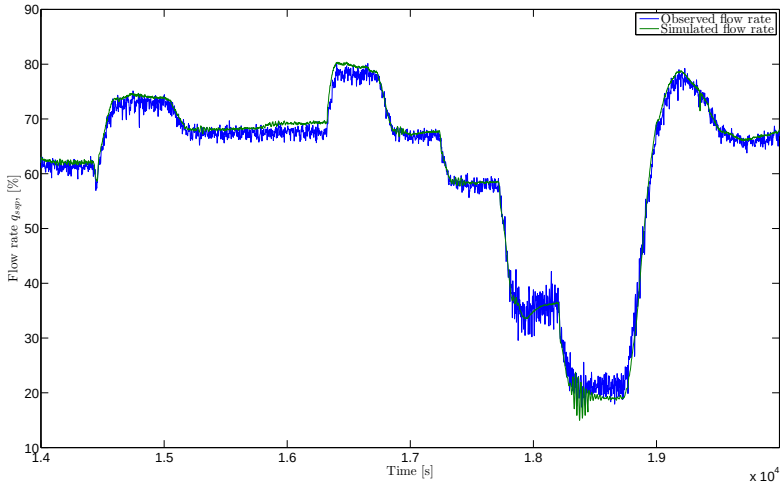

Figure 4.2: Simulation of the flow rate through the subsea pump q_{ssp}

equation in Eq. 3.46 into an implicit relationship for q_{ssp}:

$$\underbrace{\rho g \cdot (c_0 \omega_{ssp}^{n0} - c_1 \omega_{ssp} \cdot q_{ssp} - c_2 q_{ssp}^{n2})}_{\Delta P_{SPM}} = \underbrace{(B + D \cdot q_{ssp}^2 + E \cdot q_{ssp}^3)}_{F_{MRL}} + \underbrace{\rho g h_r}_{G_{tot}} \tag{4.2}$$

This implicit equation can be easily solved in MATLAB, where the solution is found by applying the build-in implicit solver `fzero.m`. The function applies the bisection method to find a root of any nonlinear expression based on an initial guess for the solution. A comprehensive description of this method is outside the scope of this thesis, but documentation of the function is readily available in MathWorks [2015b].

A MATLAB function was written to solve for the time series of q_{ssp} based on the implicit equation in Eq. 4.2. The implementation for numerical solving of the equation is omitted in the text due to its structure very similar as the implementation of the dynamic simulation.

The steady-state system is simulated for the same time horizon and for the same input variable from measurements as in the dynamic simulation. Figure 4.3 shows the simulated state variable q_{ssp} from the steady-state simulation along with the dynamical simulated output.

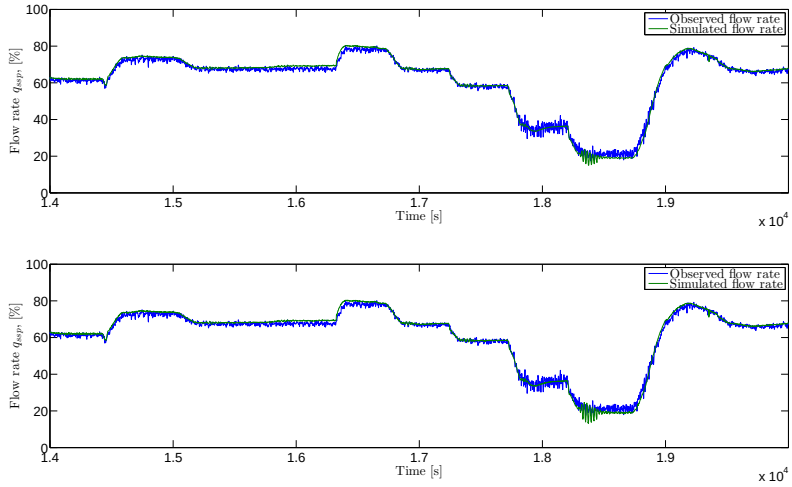

Figure 4.3: Simulation of the flow rate through the subsea pump q_{ssp} with the dynamic equation of Eq. 3.46 (above) and the static equation of Eq. 4.2 (below).

As seen from the plot, the simulated time series are in principle inseparable from one another, confirming that the dynamics in the SPM flow rate are negligible.

4.3 Simulations of Complete MRL Dynamics

Now that the dynamics of the riser level and the MRL flow rate have been simulated separately, the state equations should be simulated simultaneously to test the validity of the complete identified MRL dynamics. Similarly as for previous sections, the continuous dynamics are implemented as a MATLAB function to be solved with the `ode45()` solver. Due to the similarity with the separate dynamics implementations, `MRL_dynamics` are omitted in the text.

A MATLAB function was written to simulate the complete dynamics of Eq. 3.45 - 3.46. A figure of the observed and simulated states is shown below in Figure 4.4. Comparing with the simulations of the separate riser dynamics in Figure 4.1 and the separate flow rate dynamics in Figure 4.2, the simulation of the complete dynamics yields much more consistency between observed and simulated riser level state, but some less consistency between observed and simulated flow rate state. Due to the interconnection of the two states in one simulation, the previously large deviation from observations in the riser level state is handled by the closed-loop structure of the flow rate dynamics. The compromise is some increased inaccuracy of the simulation of the flow rate.

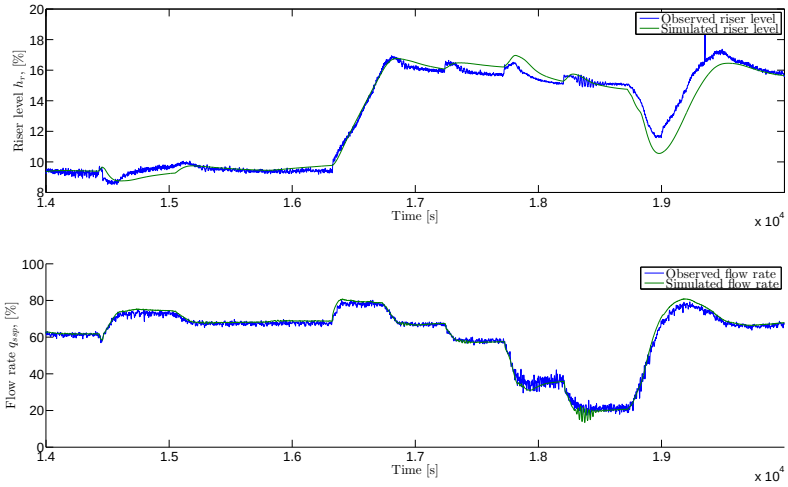

Figure 4.4: Simulation of the complete dynamics of Eq. 3.45 - 3.46.

Chapter 5

Conclusion

The aim of this thesis was to investigate a real dual gradient drilling system in the Gulf of Mexico through modeling and application of field data in order to estimate unknown parameters. Initially, a model for the complete system was derived to a large extent based on general and well-known modeling assumptions known from prior work on managed pressure drilling as well as dual gradient drilling.

In the following, system identification tools were applied to estimate the unknown parameters in the expressions for the frictional pressure losses in the mud return line and for the head of the subsea pump. Initially, both the identified models failed to replicate the observed measurements in a satisfactory manner. Also, the obtained models gave rise to several unphysical characteristics, like negative frictional losses and increasing pump head for increasing flow, which argue in favor of rejection of the models. Slight modifications to the model structures were suggested. This lead to a much improved statistical properties of the models and reasonable results.

Simulation of the system dynamics yielded state outputs that replicated the observed measurement to a satisfactory degree. It should be expected, that due to the many simplifying assumptions made in the modeling section, the identified model will not be able to reproduce a wide range of dynamic effects. Therefore, although all transient effects are not expressed by the identified system, the model can be taken as sufficiently accurate for control design and considered validated.

The main contribution of this thesis is to derive a DGD model and to validate it using system identification tools. An identified system model serves as a necessary prerequisite for experimenting with controller design and tuning. The obtained model could therefore be an important and valuable contribution to ease controller tuning offshore, which saves valuable rig time.

Bibliography

Anfinsen, H., 2012. Modelling and estimation of u-tubing effects in the low riser return system. Master's thesis, NTNU.

API, 2006. Rheology and hydraulics of oil-well drilling fluids.

Breyholtz, Ø., Nygaard, G., Nikolaou, M., 2009. Evaluating new and existing automatically controlled deep water drilling concepts using a high-fidelity simulation model. In: Proc. Scandinavian Conf. on Simulation and Modeling.

Breyholtz, Ø., Nygaard, G., Nikolaou, M., 2011. Managed pressure drilling: Using model predictive control to improve pressure control during dual-gradient drilling. SPE Drilling & Completion 26, 182–197.

Çengel, Y., Cimbala, J., 2010. Fluid Mechanics Fundamentals and Applications. McGraw Hill.

Egeland, O., Gravdahl, J., 2002. Modelling and Simulation for Automatic Control. Trondheim, Norway: Marine Cybernetics.

Fossum, T., 2013. Analysis and control of drilling riser dynamics in dual gradient drilling. Master's thesis, NTNU.

Ioannou, P., Sun, J., 2012. Robust Adaptive Control. Dover.

Isambourg, P., Anfinsen, B., Marken, C., 1996. Volumetric behavior of drilling muds at high pressure and high temperature. Paper SPE 36830 presented at European Petroleum Conference, Milan, Italy, 22-24 October.

Kaasa, G.-O., Stamnes, Ø., Imsland, L., Aamo, O., 2011. Intelligent estimation of downhole pressure using a simple hydraulic model. Paper IADC/SPE 143097 presented at IADC/SPE Managed Pressure Drilling and Underbalanced Operations Conference and Exhibition held in Denver, Colorado, USA, 5-6 April.

Landet, I., 2011. Modeling and control for managed pressure drilling from floaters. Master's thesis, NTNU.

Ljung, L., 1999. System Identification: Theory for the User. Prentice Hall.

MathWorks, 2015a. Documentation of MATLAB algorithm `fminsearch`. `http://www.mathworks.se/help/matlab/ref/fminsearch.html`, accessed: 2015-04-29.

MathWorks, 2015b. Documentation of MATLAB algorithm `fzero`. `http://www.mathworks.se/help/matlab/ref/fzero.html`, accessed: 2015-06-08.

MathWorks, 2015c. Documentation of MATLAB algorithm `lscov`. `http://www.mathworks.se/help/matlab/ref/lscov.html`, accessed: 2015-04-29.

MathWorks, 2015d. Documentation of MATLAB algorithm `ode45`. `http://www.mathworks.se/help/matlab/ref/ode45.html`, accessed: 2015-06-07.

Meritt, H., 1967. Hydraulic Control Systems. John Wiley & Sons, U.S.

Nocedal, J., Wright, S., 2006. Numerical Optimization. Springer.

Riet, E., Reitsma, D., Vandecraen, B., 2003. Development and testing of a fully automated system to accurately control downhole pressure during operations. Paper SPE/IADC 85310 presented at SPE/IADC Middle East Technology Drilling Conference and Exhibition held in Abu Dhabi, UAE, 20-22 October.

Stamnes, Ø., 2011. Nonlinear estimation with applications to drilling. Ph.D. thesis, NTNU.

Stamnes, Ø., Mjaavatten, E., Falk, K., 2012. A simplified model for multi-fluid dual gradient drilling operations. In: Proceedings of the 2012 IFAC Workshop on Automatic Control in Offshore Oil and Gas Production. pp. 211–216.

White, F., 1994. Fluid Mechanics. McGraw Hill.